Acta Crystallographica Section B
Structural Science
ISSN 0108-7681

Comparison of the effects of pressure on three layered hydrates: a partially successful attempt to predict a high-pressure phase transition

Russell D. L. Johnstone,[a] Alistair R. Lennie,[b] Simon Parsons,[a]* Elna Pidcock[c] and John E. Warren[b]

[a]School of Chemistry and Centre for Science at Extreme Conditions, The University of Edinburgh, King's Buildings, West Mains Road, Edinburgh EH9 3JJ, Scotland, [b]Synchrotron Radiation Source, STFC Daresbury Laboratory, Warrington, Cheshire WA4 4AD, England, and [c]Cambridge Crystallographic Data Centre, 12 Union Road, Cambridge CB2 1EZ, England

Correspondence e-mail: s.parsons@ed.ac.uk

Received 25 June 2009
Accepted 28 September 2009

We report the effect of pressure on the crystal structures of betaine monohydrate (BTM), L-cysteic acid monohydrate (CAM) and *S*-4-sulfo-L-phenylalanine monohydrate (SPM). All three structures are composed of layers of zwitterionic molecules separated by layers of water molecules. In BTM the water molecules make donor interactions with the same layer of betaine molecules, and the structure remains in a compressed form of its ambient-pressure phase up to 7.8 GPa. CAM contains bi-layers of L-cysteic acid molecules separated by water molecules which form donor interactions to the bi-layers above and below. This phase is stable up to 6.8 GPa. SPM also contains layers of zwitterionic molecules with the waters acting as hydrogen-bond donors to the layers above and below. SPM undergoes a single-crystal to single-crystal phase transition above 1 GPa in which half the water molecules reorient so as to form one donor interaction with another water molecule within the same layer. In addition, half of the *S*-4-sulfo-L-phenylalanine molecules change their conformation. The high-pressure phase is stable up to 6.9 GPa, although modest rearrangements in hydrogen bonding and molecular conformation occur at 6.4 GPa. The three hydrates had been selected on the basis of their topological similarity (CAM and SPM) or dissimilarity (BTM) with serine hydrate, which undergoes a phase transition at 5 GPa in which the water molecules change orientation. The phase transition in SPM shows some common features with that in serine hydrate. The principal directions of compression in all three structures were found to correlate with directions of hydrogen bonds and distributions of interstitial voids.

1. Introduction

Pressure-induced phase transitions have been observed in a number of different classes of molecular crystal structure. Simple alcohols, carboxylic acids, phenols and acetone all exhibit new high-pressure phases (Allan *et al.*, 1998, 1999, 2001, 2002; Oswald, Allan, Motherwell *et al.*, 2005; Oswald, Allan, Day *et al.*, 2005; Allan & Clark, 1999*a*,*b*). Phase transitions have also been observed in more complex materials such as amino acids (Moggach, Parsons & Wood, 2008), pharmaceuticals and energetic materials (Fabbiani & Pulham, 2006) and even in relatively large single molecule magnets (Prescimone *et al.*, 2008).

One of the motivations for work on molecular compounds at high pressure has been to understand the driving forces behind phase transitions. Packing-energy calculations based on the PIXEL method (Gavezzotti, 2005) have shown that some transitions, such as that in salicylaldoxime (Wood *et al.*, 2006), are driven by avoidance of short intermolecular repulsions. In other transitions, such as that in serine (Wood *et*

al., 2008) and serine hydrate (Johnstone *et al.*, 2008), the thermodynamic driving force is the lower volume and more efficient packing in the high-pressure form. These two driving forces can be seen as operating *via* the U and PV terms in the equation $G = U + PV - TS$.

A number of structures in which the molecules pack in layers have now been studied at high pressure. Examples include α-glycine (Dawson *et al.*, 2005), paracetamol phases (I) and (II) (Boldyreva *et al.*, 2000, 2002) and serine hydrate (Johnstone *et al.*, 2008). The layer-stacking direction is often found to be the most compressible, as closer stacking is an effective way to minimize volume. Under ambient conditions, the crystal structure of L-serine monohydrate is built up of layers of hydrogen-bonded zwitterionic serine molecules which are linked together by hydrogen bonds to water. The orientation of the water molecules is such that the donor interactions are made to different layers (Fig. 1*a*). With the application of pressure, the crystal structure undergoes a single-crystal to single-crystal phase transition, whereby the interlayer distance is reduced so that both donor interactions are made to the same layer (Fig. 1*b*). In order to enable closer stacking of the serine layers the water molecules have to re-orient, leading to a phase transition. In this paper we investigate whether the structural change seen in serine hydrate has any generality: do layered hydrates with the configuration shown in Fig. 1(*a*) always undergo a transition to a conformation like that in Fig. 1(*b*)? Can we predict high-pressure phase transitions?

We report the effect of pressure on three layered zwitterionic hydrates (the structures of the zwitterions are shown in Fig. 2). One layered hydrate, betaine monohydrate, has a structure similar to Fig. 1(*b*). On the basis of the results on serine hydrate this was expected to be stable with respect to a Fig. 1(*a*) structure. *S*-4-Sulfo-L-phenylalanine monohydrate has a structure analogous to Fig. 1(*a*), and we expected this to be unstable with respect to Fig. 1(*b*) on compression. L-Cysteic acid monohydrate has a structure like that in Fig. 1(*a*), but with the L-cysteic acid molecules forming a bi-layer arrangement. This compound was investigated to determine whether pressure would be 'taken up' by the bi-layers or the water layers.

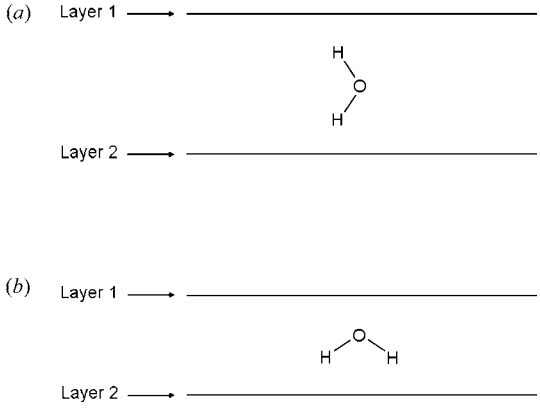

Figure 1
Orientation of the water molecules between the layers of serine in L-serine monohydrate for (*a*) ambient-pressure phase and (*b*) high-pressure phase.

2. Experimental

2.1. Crystal growth

Betaine monohydrate ('BTM', 99% purity) was purchased from Sigma–Aldrich (CAS number 590-47-6). The crystals were of sufficient size and quality to be used as received. L-Cysteic acid monohydrate ('CAM', 99% purity) was purchased from Sigma–Aldrich (CAS number 23537-25-9). A sample (0.3897 g) was dissolved in deionized water (5 ml) and ethanol was added dropwise until crystals started to form. These were then allowed to develop into large colourless rods at room temperature over a period of a few hours. *S*-4-Sulfo-L-phenylalanine monohydrate ('SPM') was synthesized and recrystallized using the method described by Xie *et al.* (2002). The resulting crystals had the appearance of colourless, elongated hexagons. For the high-pressure experiments, a crystalline sample of each hydrate was taken and loaded into a diamond–anvil cell.

2.2. Determination of ambient-pressure structures

The crystal structures of all three systems were determined at ambient pressure and temperature. The crystal used in each case was taken from the same batch as the sample used for the corresponding compression study. Data were measured on a Bruker SMART APEX diffractometer with graphite-monochromated Mo $K\alpha$ radiation (λ = 0.71073 Å) at 293 K. The data were integrated using *SAINT* (Bruker–Nonius, 2006) and corrected for absorption with *SADABS* (Sheldrick, 2004). Data were merged in point groups *mmm*, 222 and 2 for BTM, CAM and SPM.

Structures were solved using the program *SIR*92 (Altomare *et al.*, 1994) and were refined against $|F|^2$ using all data (*CRYSTALS*; Betteridge *et al.*, 2003). All non-H atoms were refined with anisotropic displacement parameters. H atoms attached to carbon and nitrogen were placed geometrically and constrained to ride on their host atoms. H atoms attached to O atoms were found in Fourier difference maps, and their positions were refined subject to an O—H distance restraint of

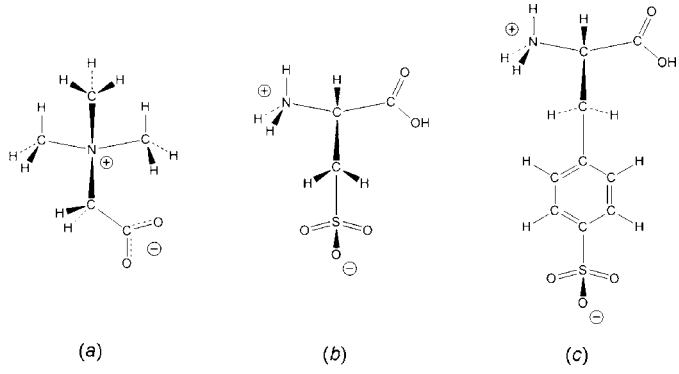

Figure 2
Molecular structures of (*a*) betaine, (*b*) L-cysteic acid and (*c*) *S*-4-sulfo-L-phenylalanine.

Table 1
Crystallographic data for betaine monohydrate at increasing pressures.

λ = 0.71073 Å for the ambient-pressure data set and 0.4762 Å for the high-pressure data sets. Experiments were carried out at 293 K. Absorption was corrected for by multi-scan methods, *SADABS* (Siemens, 1996). Full tables of crystallographic data for all pressures have been deposited as supplementary material.

Pressure (GPa)	Ambient	7.8
Crystal data		
Chemical formula	$C_5H_{13}NO_3$	$C_5H_{13}NO_3$
M_r	135.16	135.16
Crystal system, space group	Orthorhombic, *Pbca*	Orthorhombic, *Pbca*
a, b, c (Å)	9.4715 (4), 11.4963 (5), 13.0802 (6)	8.778 (2), 10.656 (4), 11.884 (3)
V (Å)	1424.27 (11)	1111.7 (6)
Z	8	8
D_x (Mg m^{-3})	1.261	1.615
Radiation type	Mo $K\alpha$	Synchrotron
μ (mm^{-1})	0.10	0.13
Crystal shape, colour	Block, colourless	Block, colourless
Crystal size (mm)	0.85 × 0.55 × 0.46	0.20 × 0.20 × 0.10
Data collection		
Diffractometer	Bruker APEX	Bruker APEX-II
T_{min}, T_{max}	0.80, 0.95	0.67, 0.99
No. of measured, independent and observed [$I > 2.0\sigma(I)$] reflections	14 918, 1909, 1761	2684, 252, 187
R_{int}	0.047	0.129
d_{max}, d_{min} (Å)	6.54, 0.72	5.94, 1.10
θ_{max} (°)	29.6	12.6
Refinement		
Refinement on	F^2	F
$R[F^2 > 2\sigma(F^2)]$, $wR(F^2)$, S	0.064, 0.153, 1.08	0.100, 0.135, 1.02
No. of reflections	1909	187
No. of parameters	89	41
No. of restraints	2	126
$(\Delta/\sigma)_{max}$	< 0.0001	< 0.0001
$\Delta\rho_{max}$, $\Delta\rho_{min}$ (e Å^{-3})	0.34, −0.23	0.60, −0.61
Completeness	95.1% (0.7 Å)	55.8% (1.0 Å)
Extinction method	Larson (1970), equation (22)	None
Extinction coefficient	0.660 (6)	–

0.84 (1) Å. Isotropic displacement parameters were refined for H atoms attached to oxygen; those on the water molecules were constrained to be equal. Listings of crystal and refinement data are given in Tables 1–3.[1] Displacement ellipsoid plots with atomic numbering schemes are shown in Figs. 3(*a*)–(*c*).

2.3. High-pressure crystallography: data processing and general procedures

High-pressure experiments were carried out using a Merrill–Bassett diamond–anvil cell (half-opening angle 40°), equipped with Boehler–Almax cut diamonds with 600 µm culets and a tungsten gasket (Merrill & Bassett, 1974; Moggach, Allan *et al.*, 2008).

For each pressure study, a 1:1 mixture of *n*-pentane and isopentane was used as a hydrostatic medium. This hydrostatic medium is very volatile and so the cell was cooled in dry ice prior to loading. A small ruby chip was also loaded into the cell as the pressure callibrant, and the ruby fluorescence method used to measure the pressure (Piermarini *et al.*, 1975).

All diffraction data were collected on a Bruker–Nonius APEX-II diffractometer with silicon-monochromated synchrotron radiation (λ ≃ 0.48 Å, see Tables 1–3) on Station 9.8 at the SRS, Daresbury Laboratory. Data collection and processing procedures for all the high-pressure experiments followed Dawson *et al.* (2004). Integrations were carried out using dynamic masking of the regions of the detector shaded by the pressure cell with the program *SAINT*. An absorption correction was carried out in a two-stage procedure with the programs *SHADE* (Parsons, 2004) and *SADABS*. Data were merged using *SORTAV* (Blessing, 1987) in point groups *mmm*, *mmm* and 2/*m* for BTM, CAM and SPM. In each study, pressure was increased in regular steps until either the limit of the hydrostatic medium was reached or peak broadening became too severe for further data collection.

Inspection of the unit-cell constants for BTM and CAM upon compression to 7.8 and 6.8 GPa showed that both remain in compressed forms of their respective ambient-pressure phases. Compression of the ambient-pressure form of SPM (SPM-I) to 2.5 GPa resulted in a single-crystal to single-crystal phase transition to a new phase, hereafter designated SPM-II. Further compression of SPM-II revealed that a more subtle structural change occurs between 6.5 and 6.9 GPa, which resulted in a shortening of the *c* axis and a lengthening in *b*.

2.4. High-pressure crystallography: refinement

The starting coordinates of the compressed forms of BTM, CAM and SPM-I were taken from those determined at ambient pressure, and the structure of SPM-II was solved using *SIR*2004 (Burla *et al.*, 2005). All high-pressure refinements were carried out against F using data with $F > 4\sigma(F)$ in *CRYSTALS* (Betteridge *et al.*, 2003). Extreme outlier reflections (*e.g.* those partially cut-off by the pressure cell, or overlapping with diamond reflections) were omitted from the refinement.

Owing to the low completeness of the datasets (Tables 1–3), all primary bond distances and angles were restrained to the values observed at ambient-pressure conditions. In most cases, non-H atoms were refined with anisotropic displacement parameters, although for some of the higher-pressure datasets

[1] Supplementary data for this paper are available from the IUCr electronic archives (Reference: WS5073). Services for accessing these data are described at the back of the journal.

[BTM (7.8 GPa), CAM (6.8 GPa) and all structures of SPM-II] the C, N and O atoms were refined isotropically. Global rigid-bond and rigid-body restraints were applied to all anisotropic displacement parameters.

H atoms attached to C and N were placed geometrically and constrained to ride on their host atoms. H atoms attached to carboxylic acid groups were found in Fourier difference maps and their positions were refined subject to an O—H distance restraint of 0.84 (1) Å, and a ∠COH angle restraint based on the corresponding ambient-pressure structure. Ambient-pressure structures suggested that the carboxylic acid (CCOOH) groups were planar, and so a restraint was used to enforce this in high-pressure refinements.

Water molecules were treated as rigid bodies: O—H distances were set at 0.84 Å and ∠OHO angles were constrained to be equal to those observed at ambient conditions; the orientations of the water molecules were allowed to pivot about the O-atom positions. In addition to this, restraints were applied to ensure that the water O—H bonds were directed along hydrogen-bonding vectors formed at ambient conditions [$\angle(D\mathrm{H}\cdots A) = 180\ (4)^\circ$].

Table 2
Crystallographic data for L-cysteic acid monohydrate at increasing pressures.

λ = 0.71073 Å for the ambient-pressure data set and 0.4762 Å for the high-pressure data sets. Full tables of crystallographic data for all pressures have been deposited as supplementary material.

Pressure (GPa)	Ambient	6.8
Crystal data		
Chemical formula	$C_3H_9NO_6S$	$C_3H_9NO_6S$
M_r	187.17	187.17
Crystal system, space group	Orthorhombic, $P2_12_12_1$	Orthorhombic, $P2_12_12_1$
a, b, c (Å)	6.9233 (2), 19.0222 (5), 5.3030 (2)	6.4885 (14), 17.834 (7), 5.0983 (13)
V (Å)	698.39 (4)	590.0 (3)
Z	4	4
D_x (Mg m^{-3})	1.780	2.107
Radiation type	Mo $K\alpha$	Synchrotron
μ (mm^{-1})	0.45	0.53
Crystal shape, colour	Rod, colourless	Rod, colourless
Crystal size (mm)	0.20 × 0.20 × 0.10	0.20 × 0.20 × 0.10
Data collection		
Diffractometer	Bruker APEX	Bruker APEX-II
T_{min}, T_{max}	0.68, 0.84	0.68, 0.95
No. of measured, independent and observed [$I > 2.0\sigma(I)$] reflections	7112, 1129, 1816	1508, 183, 139
R_{int}	0.026	0.092
d_{max}, d_{min} (Å)	9.51, 0.72	6.10, 0.90
θ_{max} (°)	29.6	15.3
Refinement		
Refinement on	F^2	F
$R[F^2 > 2\sigma(F^2)]$, $wR(F^2)$, S	0.032, 0.044, 1.20	0.078, 0.093, 0.92
No. of reflections	1834	139
No. of parameters	111	58
No. of restraints	3	149
$(\Delta/\sigma)_{max}$	< 0.0001	< 0.0001
$\Delta\rho_{max}$, $\Delta\rho_{min}$ (e Å^{-3})	0.27, −0.59	0.36, −0.30
Completeness	95.6% (0.7 Å)	34.2% (0.90 Å)
Extinction method	Larson (1970) equation 22	None
Extinction coefficient	0.588 (6)	–
Absolute structure	Flack (1983)	As ambient
Flack parameter	0.056 (6)	–

The positions of the water H atoms in SPM-II were just visible in a Fourier-difference map, and were confirmed using a maximum entropy-enhanced difference map calculated using the program *BAYMEM* (van Smaalen *et al.*, 2003). Isotropic displacement parameters for all O—H H atoms were refined subject to restraints and those attached to the water oxygen atom were constrained to be equal. Planarity restraints were applied to the phenyl rings in all structures of SPM-II. Refinements were weighted using a Chebychev polynomial function as described in Watkin (1994) with a robust-resistant modifier (Prince, 1982). Listings of crystal and refinement data are given in Tables 1–3; intermolecular interactions are given in Tables 4–6.

2.5. PIXEL calculations

The final crystal structures obtained were used to calculate in separate calculations the molecular electron densities of the zwitterion and water molecules at each pressure by standard quantum-chemical methods using the program *GAUSSIAN*98 (Frisch *et al.*, 1998) with the MP2/6-31G** basis set. The calculations are sensitive to H-atom positions (which become difficult to determine especially at higher pressures), and H-atom distances were set to standard neutron values in all calculations (C—H = 1.083 Å, N—H = 1.009 Å, O—H = 0.983 Å). The electron-density model of the molecule was then analysed using the program package *OPiX* (Gavezzotti, 2003), which allows the calculation of dimer and lattice energies. The output from these calculations yields a total energy and a breakdown into its Coulombic (electrostatic), polarization, dispersion and repulsion components (Gavezzotti, 2005, 2007).

2.6. Other programs used

Crystal structures were visualized using the programs *CAMERON* (Watkin *et al.*, 1993), *Materials Mercury* (Macrae *et al.*, 2008), *XP* (Sheldrick, 2005) and *DIAMOND* (Brandenburg & Putz, 2005). Void diagrams were created in *Mercury* and are shown with a probe radius of 0.2 Å and a default grid spacing of 1 Å. Analyses were carried out using *PLATON* (Spek, 2004), as incorporated in the *WinGX* suite (Farrugia, 1999). Searches of the Cambridge Structural Database (CSD; Allen & Motherwell, 2002) utilized the program *CONQUEST* with database updates up to November

Table 3
Crystallographic data for *S*-4-sulfo-L-phenylalanine monohydrate at increasing pressures.

λ = 0.71073 Å for the ambient-pressure data set and 0.4762 Å for the high-pressure data sets. Full tables of crystallographic data for all pressures have been deposited as supplementary material.

Pressure (GPa)	Ambient	1.0	2.5	6.9
Phase	(I)	(I)	(II)	(II)
Crystal data				
Chemical formula	$C_9H_{13}NO_6S$	$C_9H_{13}NO_6S$	$C_9H_{13}NO_6S$	$C_9H_{13}NO_6S$
M_r	263.27	263.27	263.27	263.27
Crystal system, space group	Monoclinic, $P2_1$	Monoclinic, $P2_1$	Monoclinic, $P2_1$	Monoclinic, $P2_1$
a, b, c (Å)	6.5299 (5), 7.6432 (6), 11.6081 (9)	6.3782 (3), 7.4754 (3), 11.4450 (13)	10.2176 (8), 8.2463 (5), 12.6853 (17)	9.5437 (17), 8.1824 (12), 12.151 (4)
β (°)	93.590 (5)	92.591 (7)	114.238 (9)	111.30 (2)
V (Å)	578.22 (8)	545.14 (7)	974.61 (18)	884.0 (4)
Z	2	2	4	4
D_x (Mg m^{-3})	1.512	1.604	1.794	1.978
Radiation type	Mo $K\alpha$	Synchrotron	Synchrotron	Synchrotron
μ (mm^{-1})	0.30	0.32	0.35	0.39
Crystal shape, colour	Hexagon, colourless	Hexagon, colourless	Hexagon, colourless	Hexagon, colourless
Crystal size (mm)	0.65 × 0.40 × 0.20	0.20 × 0.20 × 0.10	0.20 × 0.20 × 0.10	0.20 × 0.20 × 0.10
Data collection				
Diffractometer	Bruker APEX	Bruker APEX	Bruker APEX	Bruker APEX-II
T_{min}, T_{max}	0.80, 0.94	0.72, 0.97	0.81, 0.97	0.64, 0.96
No. of measured, independent and observed [$I > 2.0\sigma(I)$] reflections	7731, 1775, 2784	3231, 561, 499	4262, 786, 594	1921, 351, 269
R_{int}	0.033	0.046	0.071	0.150
d_{max}, d_{min} (Å)	11.58, 0.70	4.41, 0.70	9.37, 0.80	8.70, 1.00
θ_{max} (°)	30.5	20.0	17.4	13.6
Refinement				
Refinement on	F^2	F	F	F
$R[F^2 > 2\sigma(F^2)]$, $wR(F^2)$, S	0.053, 0.056, 1.18	0.029, 0.027, 0.88	0.068, 0.067, 0.95	0.111, 0.126, 0.74
No. of reflections	2999	499	594	269
No. of parameters	165	162	163	163
No. of restraints	4	402	463	
$(\Delta/\sigma)_{max}$	< 0.0001	< 0.0001	< 0.0001	< 0.0001
$\Delta\rho_{max}$, $\Delta\rho_{min}$ (e Å^{-3})	0.65, −0.50	0.10, −0.11	0.31, −0.30	0.46, −0.46
Completeness	93.5% (0.7 Å)	31.7% (0.7 Å)	36.8% (0.8 Å)	36.6% (1.0 Å)
Absolute structure	(Flack, 1983)	As ambient	As ambient	As ambient
Flack parameter	0.030 (11)	–	–	–

2008. Calculations of strain tensors were carried out using a locally written program (Parsons, 2003) using the method described in Hazen & Finger (1982). Eigenvalues and vectors were calculated using the *JACOBI* routine in *Numerical Recipes* (Press *et al.*, 1992).

3. Results

3.1. Structure of betaine monohydrate at ambient pressure

The crystal structure of BTM contains one formula unit in the asymmetric unit in the space group *Pbca*, and corresponds to a structure determined previously by Mak (1990). The betaine molecule is zwitterionic with negative charge localized around the carboxylate group and positive charge residing on the quaternary N atom. Betaine has approximate C_S point symmetry: a least-squares mean plane through the atoms C3, N1, C4, C5, O2 and O1 shows that the average deviation from the plane is 0.016 Å (Fig. 3*a*).

The structure comprises layers of betaine molecules which lie parallel to the (010) plane (Fig. 4*a*). PIXEL calculations indicate that the betaine molecules within each layer interact *via* Coulombic attractions between oppositely charged parts of each zwitterion and also by dispersion attractions. Both the betaine and water layers are slightly sinusoidal when viewed along the *a* axis; a feature emphasized by the colour-coding in Fig. 4(*b*).

The water molecules reside between the betaine layers (Fig. 4*c*) and they interact with the layers through two hydrogen bonds (Table 4). Each hydrogen bond is donated to carboxylate O atoms on different molecules in a single layer (Fig. 4*a*), forming chains of the graph-set descriptor $C(6)$ (Bernstein *et al.*, 1995) which run parallel to the *a* axis (Figs. 4*a* and *c*). There are no geometrically favourable CH···O contacts formed to the water molecules at ambient pressure.

3.2. Compression of betaine monohydrate

Increasing pressure on BTM produces an anisotropic response in the unit-cell parameters (Fig. 5*a*). The crystal system is orthorhombic, and the principal axes of the strain tensor coincide with the crystallographic axes (Table 7).

Although layered structures are often found to compress most along the layer stacking direction, this is not the case here: the greatest reduction occurs along the *c* axis (parallel to the layers), which decreases by 9.1% from ambient conditions to 7.8 GPa. The *a* and *b* axes are equally compressible (both shortening by 7.3%). The molecular volume reduces by 21.9% at 7.8 GPa with respect to ambient conditions (Fig. 5*b*).

The curves of the *a* and *c* axes appear to flatten out at 6.6 GPa; the *c* axis even appears to start to increase slightly from 6.6 to 7.8 GPa. The *b* axis does not reach a minimum at high pressure and continues to decrease throughout; the rate of compression between layers does not appear to change much from 1.6 to 7.8 GPa.

As pressure is increased, the betaine molecules distort from C_S point symmetry as the carboxylate group twists about the C4—C5 vector; the largest change in non-H torsion angle occurs in N1—C4—C5—O1 which changes by *ca* 9° from ambient to 7.8 GPa. The average deviation from the least-squares mean plane defined by atoms C3, N1, C4, C5, O2 and O1 is approximately three times that seen at ambient conditions (0.053 Å).

The two hydrogen bonds in the structure shorten by *ca* 6% at 7.8 GPa relative to ambient conditions (Table 4).

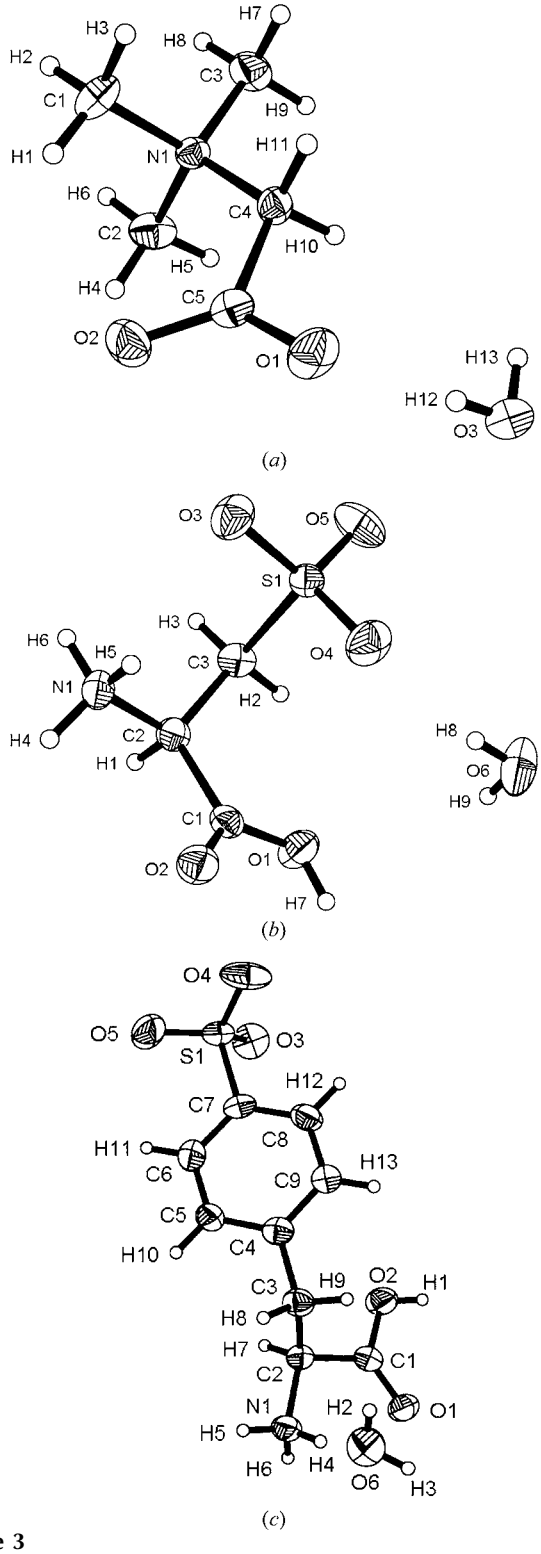

Figure 3
The asymmetric unit of (*a*) betaine monohydrate, (*b*) L-cysteic acid monohydrate and (*c*) *S*-4-sulfo-L-phenylalanine monohydrate at ambient pressure and room temperature. Ellipsoids encompass 30% probability surfaces.

3.3. Structure of L-cysteic acid monohydrate at ambient pressure

The crystal structure of CAM has previously been determined by Ramanadham *et al.* (1973); there is one formula unit in the asymmetric unit and the space group is $P2_12_12_1$. Molecules of L-cysteic acid are zwitterionic: the amino group extracts a H atom from the sulfonate moiety leaving the carboxyl group protonated (Fig. 3*b*).

The structure is made up of bi-layers of L-cysteic acid molecules which lie parallel to the (010) plane (Fig. 6*a*). The bi-layers are formed by three hydrogen bonds (Table 5, Fig. 6*a*), each donated from the ammonium group: two are accepted by sulfonate O atoms in different molecules (N1H5···O3 and N1H6···O3) which together form *C*(4) chains along the *c* axis; another is accepted by the unprotonated carboxyl oxygen (N1H4···O2).

Water molecules lie between the bi-layers (Fig. 6*b*). The orientation of the water molecules with respect to the layers is similar to the form shown in Fig. 1(*a*), so that the bi-layers are connected along the *b* axis through hydrogen bonds involving the water molecules. The water molecules form hydrogen bonds *via* their donor atoms to sulfonate groups in the layers above and below (O6H8···O4 and O6H9···O5). Each water molecule also accepts a hydrogen bond from the carboxylic acid group (O1H7···O6).

3.4. Compression of L-cysteic acid monohydrate

The reduction in the *a* and *b* axes as pressure is increased is more or less the same (Fig. 7*a*); both shortening by *ca* 6% upon compression from ambient conditions to 6.8 GPa. As in the compression of BTM, the graphs showing the reduction in the layer-building (*a* and *c*) axes flatten out at high pressure, whereas the graph for the layer stacking axis (*b*) does not, and continues to decrease throughout the pressure range. The

Table 4
Non-covalent parameters in the crystal structure of betaine monohydrate up to 7.8 GPa.

All distances are given in Å and angles are given in °. S.u.s are calculated in *PLATON*; H-atom positions were as obtained from the refinement and *X*—H have not been normalized to neutron values.

Pressure (GPa)	0	0.1	1.6	2.9	4.0	4.9
O3H12···O1^{i}						
H12···O1	1.98 (2)	1.97 (2)	1.93 (3)	1.89 (2)	1.88 (3)	1.87 (3)
O3···O1	2.814 (2)	2.806 (4)	2.764 (3)	2.730 (3)	2.717 (3)	2.700 (3)
∠O3H12O1	176 (2)	173 (2)	174 (3)	174 (2)	174 (3)	173 (3)
O3H13···O2^{ii}						
H13···O2	1.95 (2)	1.94 (2)	1.90 (2)	1.87 (2)	1.86 (2)	1.84 (2)
O3···O2	2.782 (2)	2.778 (4)	2.728 (4)	2.705 (4)	2.686 (4)	2.672 (4)
∠O3H13O2	169 (2)	173 (2)	170 (2)	172.5 (18)	170 (3)	168 (3)

Pressure (GPa)	5.6	6.1	6.6	7.1	7.8
O3H12···O1^{i}					
H12···O1	1.86 (3)	1.83 (2)	1.83 (3)	1.84 (3)	1.83 (3)
O3···O1	2.694 (3)	2.680 (3)	2.665 (3)	2.677 (5)	2.644 (13)
∠O3H12O1	175 (3)	175 (3)	174 (4)	175 (6)	175 (4)
O3H13···O2^{ii}					
H13···O2	1.84 (2)	1.83 (2)	1.82 (2)	1.84 (3)	1.78 (3)
O3···O2	2.665 (4)	2.656 (4)	2.642 (4)	2.634 (6)	2.611 (14)
∠O3H13O2	169 (3)	169 (3)	170 (3)	166 (3)	168 (4)

Symmetry codes: (i) x, y, z; (ii) $\frac{1}{2}+x, y, \frac{1}{2}-z$.

Table 5
Non-covalent parameters in the crystal structure of L-cysteic acid monohydrate up to 6.8 GPa.

All distances are given in Å and angles are given in °. S.u.s are calculated in *PLATON*; H-atom positions were as obtained from the refinement and *X*—H have not been normalized to neutron values.

Pressure (GPa)	0	0.2	1.2	2.8	4.5	5.8	6.8
Bi-layer forming hydrogen bonds							
N1H4···O2^{i}							
H4···O2	2.08	2.09	2.08	2.04	2.02	2.01	1.96
N1···O1	2.820 (2)	2.824 (5)	2.796 (5)	2.735 (5)	2.699 (6)	2.670 (8)	2.628 (16)
∠N1H4O2	138	137	135	132	130	128	129
N1H5···O3^{ii}							
H5···O3	2.16	2.15	2.09	2.02	1.97	1.92	1.93
N1···O3	2.964 (2)	2.949 (4)	2.894 (4)	2.824 (4)	2.771 (4)	2.724 (6)	2.742 (13)
∠N1H5O3	147	147	146	146	146	146	148
N1H6···O3^{iii}							
H6···O3	2.04	2.04	2.03	2.01	1.99	1.99	1.97
N1···O3	2.944 (2)	2.943 (4)	2.932 (4)	2.907 (4)	2.891 (4)	2.878 (6)	2.849 (13)
∠N1H6O3	174	174	173	170	168	165	163
Hydrogen bonds between the water and cysteic acid layers							
O1H7···O6^{iv}							
H···O6	1.674 (17)	1.699 (18)	1.677 (18)	1.655 (17)	1.650 (17)	1.641 (15)	1.64 (2)
O1···O6	2.515 (2)	2.530 (4)	2.509 (4)	2.492 (4)	2.488 (4)	2.472 (5)	2.472 (14)
∠O1H7O6	176 (2)	173 (3)	170 (3)	174 (2)	176 (2)	169 (3)	171 (3)
O6H8···O4^{v}							
H8···O4	2.014 (16)	1.984 (16)	1.934 (16)	1.870 (12)	1.824 (13)	1.78 (2)	1.79 (3)
O6···O4	2.819 (2)	2.812 (8)	2.767 (6)	2.699 (6)	2.653 (7)	2.614 (8)	2.62 (2)
∠O6H8O4	165 (3)	168 (2)	171 (3)	168 (2)	169 (2)	170 (3)	170 (3)
O6H9···O5^{vi}							
H9···O5	1.99 (2)	1.98 (2)	1.95 (2)	1.92 (2)	1.90 (2)	1.88 (2)	1.90 (3)
O6···O5	2.790 (2)	2.785 (5)	2.755 (5)	2.731 (5)	2.708 (6)	2.679 (7)	2.702 (18)
∠O6H9O5	160 (2)	160 (2)	160 (2)	161 (2)	160 (2)	159 (2)	160 (3)

Symmetry codes: (i) $-\frac{1}{2}-x, 1-y, -\frac{1}{2}+z$; (ii) $\frac{1}{2}-x, 1-y, \frac{1}{2}+z$; (iii) $\frac{1}{2}-x, 1-y, -\frac{1}{2}+z$; (iv) $-\frac{1}{2}+x, \frac{1}{2}-y, 2-z$; (v) x, y, z; (vi) $-\frac{1}{2}+x, \frac{1}{2}-y, 1-z$.

molecular volume decreases by 15.5% from ambient conditions to 6.8 GPa (Fig. 7*b*).

The molecular geometry of the L-cysteic acid molecules remains essentially unchanged upon compression: the largest change in torsion angle involving non-H atoms is in the carboxyl group along the C1—C2 bond: O1—C1—C2—N1 changes by *ca* 4°. Overall, at ambient conditions the hydrogen bonds which form the bi-layers are longer than those formed between bi-layers and water molecules (Table 5), and on average they compress slightly more. The most compressible hydrogen bond is N1H5···O3 (the longest at ambient conditions) and shortens by 7.5%. The least compressible hydrogen bond is O1H7···O6 (the shortest at ambient conditions) which shortens by 1.7% up to 6.8 GPa to become particularly short [O···O = 2.472 (14) Å].

3.5. Structure of *S*-4-sulfo-L-phenylalanine monohydrate (I) at ambient pressure

The crystal structure of SPM-I contains one formula unit in the asymmetric unit, and crystallizes in the space group $P2_1$. The *S*-4-sulfo-L-phenylalanine molecule is zwitterionic and as in CAM, it is the sulfonate group (rather than a carboxylic acid group) which is de-protonated (Fig. 3*c*). The S1—O5 bond is almost co-planar with the plane of the phenyl ring [τ(O5—S1— C7—C6) = 11.6 (3)°], and at the other end of the molecule, the C2—C3 bond is almost perpendicular to the plane of the ring [τ(C5—C4—C3—C2) = 74.3 (3)°].

Overall the structure is made up of layers of *S*-4-sulfo-L-phenylalanine molecules which lie parallel to the (001) plane. The layers are built from two discrete hydrogen bonds: N1H5···O3 and O2H1···O4 (Table 6). A figure depicting the layers proves to be rather cluttered, and in Fig. 8(*a*) we have chosen to show only part of each molecule and one of the *C*(9) chains, running in the [110] direction. The remaining halves of the molecules generate another *C*(9) chain running along [$\bar{1}$10].

Water molecules are located between the layers with an orientation similar to Fig. 1(*a*). Layers are linked together *via* hydrogen bonding to the water of crystallization (Fig. 9*a*). Water molecules accept two hydrogen bonds from ammonium groups in layers above and below (N1H6···O6 and N1H4···O6), and donate two hydrogen bonds to sulfonate O atoms also in layers above and below (O6H2···O4 and O6H3···O2).

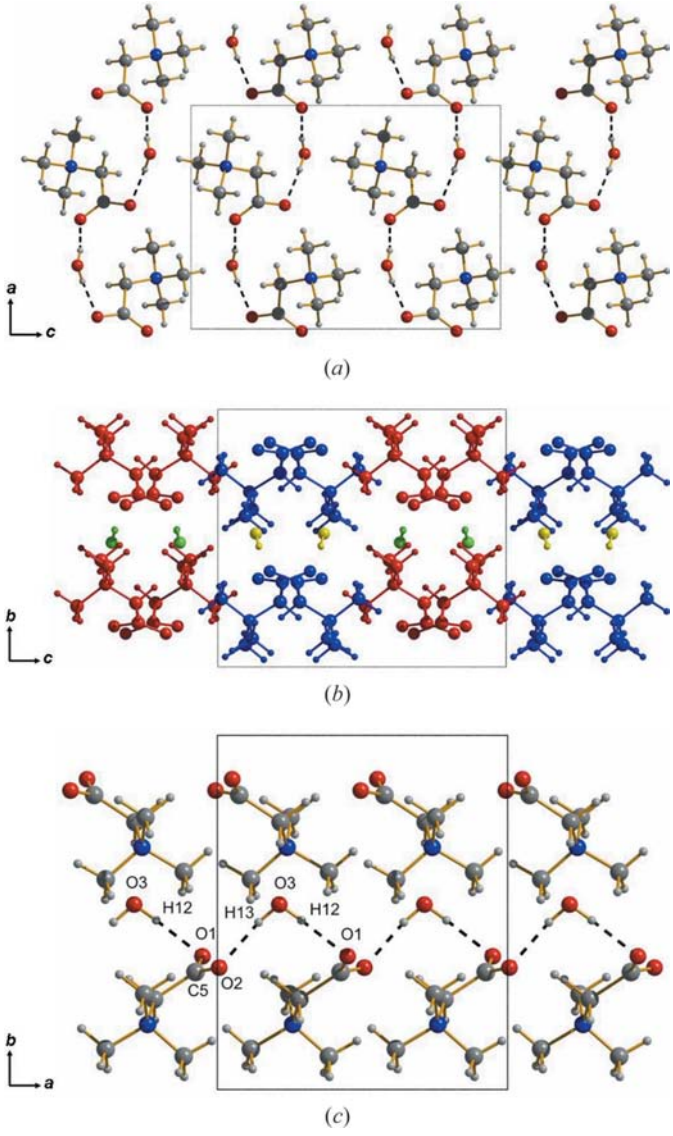

Figure 4
(*a*) One layer of betaine molecules viewed along the *b* axis; betaine molecules interact with each other *via* coulombic and dispersive interactions and with molecules in the water layer by hydrogen bonding. (*b*) Layers of betaine are sinusoidal and are separated by sinusiodal layers of water molecules. The colouring is intended to emphasize the sinusoidal arrangement of the molecules and does not imply crystallographic inequivalence. (*c*) Hydrogen bonds are formed to layers *via* water molecules (only half a unit cell along *c* is shown for clarity).

3.6. Response of *S*-4-sulfo-L-phenylalanine monohydrate (I) to compression, and the structure of *S*-4-L-phenylalanine monohydrate (II) at 2.5 GPa

The response of SPM-I to hydrostatic pressure is anisotropic (Fig. 10). The greatest reduction in the unit-cell axes occurs along *a*, which shortens by 2.3% at 1.0 GPa relative to ambient pressure, however, the direction of greatest linear strain lies along [0.13 0.00 −0.04], with other components in the stacking and layer directions (Table 7). From ambient conditions to 1.0 GPa, the interlayer separation reduces by 0.15 Å (Fig. 11).

Above 1.0 GPa, a single-crystal to single-crystal transition to a new phase (SPM-II) occurred. The structure remains in $P2_1$, but now contains two formula units in the asymmetric unit. Crystallographic data for both phases of SPM are given in Table 3. Interestingly, the inter-layer distance *increases* by 0.13 Å as the transition occurs, to become almost equal to that seen at ambient conditions in phase (I) (Fig. 11).

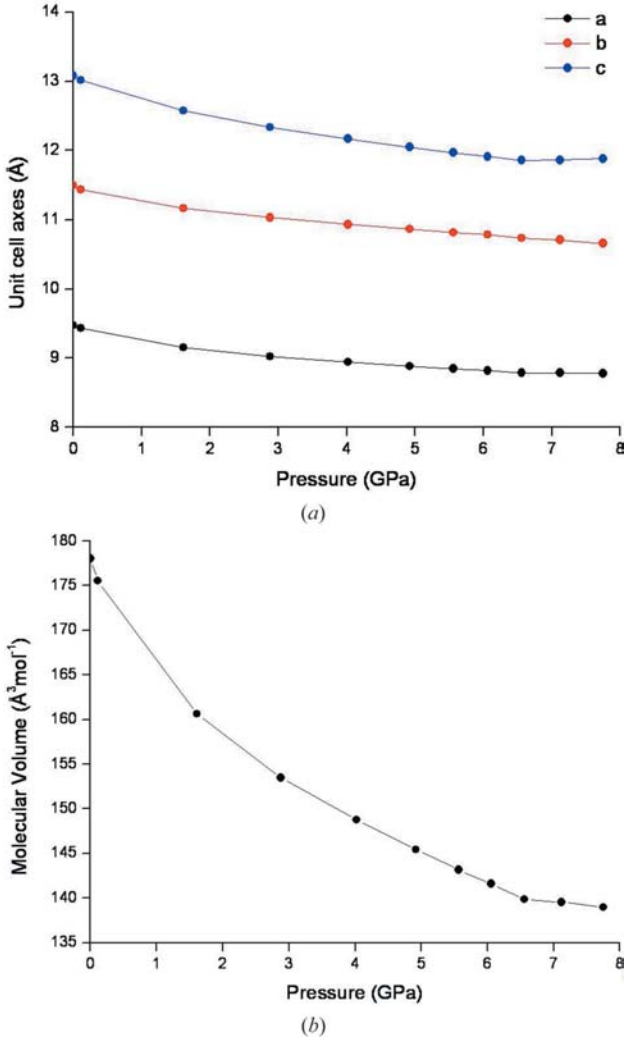

Figure 5
(*a*) Unit-cell axes for betaine monohydrate with increasing pressure. (*b*) Molecular volume of betaine monohydrate with increasing pressure.

Table 6
Non-covalent parameters in *S*-4-sulfo-L-phenylalanine monohydrate up to 6.9 GPa.

Distances are given in Å and angles are in °. S.u.s are calculated in *PLATON*; H-atom positions were as obtained from the refinement and *X*—H have not been normalized to neutron values.

Pressure (GPa)	0	0.2	1.0		2.5	4.0
Phase	(I)	(I)	(I)		(II)	(II)
Water–layer hydrogen bonds						
O6H2···O4^{i}				O61H21···O31^{iii}		
H2···O4	2.11 (3)	2.10 (2)	2.02 (2)	H21···O31	2.04 (4)	2.02 (3)
O6···O4	2.950 (3)	2.922 (6)	2.852 (6)	O61···O31	2.811 (16)	2.788 (13)
∠O6H2O4	176 (3)	168 (2)	171 (2)	∠O61H21O31	152 (4)	152 (3)
				O62H22···O52^{v}		
				H22···O52	2.01 (3)	2.00 (2)
				O62···O52	2.813 (17)	2.800 (15)
				∠O62H22O52	159 (2)	160 (3)
O6H3···O4^{ii}				O61H31···O51^{vi}		
H3···O4	2.39 (3)	2.33 (4)	2.28 (3)	H31···O51	2.22 (3)	2.14 (3)
O6···O4	3.134 (3)	3.104 (6)	3.055 (6)	O61···O51	2.980 (18)	2.900 (15)
∠O6H3O4	149 (3)	154 (2)	154 (2)	∠O61H31O51	152 (2)	151 (2)
Water–water hydrogen bonds						
				O62H32...O61^{vii}		
				H32···O61	2.10 (3)	2.15 (3)
				O62···O61	2.905 (13)	2.954 (11)
				∠O62H32O61	160 (4)	160 (4)
Layer–water hydrogen bonds						
N1H4···O6^{iii}				N11H41···O61^{viii}		
H4···O6	2.07	2.07	2.03	H41···O61	1.85	1.86
N1···O6	2.906 (3)	2.901 (5)	2.841 (4)	N11···O61	2.728 (19)	2.733 (15)
∠N1H4O6	152	151	148	∠N11H41O61	161	159
				N12H42···O62^{ix}		
				H42···O62	1.94	1.95
				N12···O62	2.817 (14)	2.830 (12)
				∠N12H42O62	163	163
N1H6···O6^{iv}				N11H61···O62^{ix}		
H6···O6	2.05	2.04	1.99	H61···O62	1.94	1.90
N1···O6	2.940 (3)	2.929 (5)	2.880 (4)	N11···O62	2.792 (16)	2.741 (14)
∠N1H6O6	164	164	164	∠N11H61O62	155	154
Layer–layer hydrogen bonds						
				N12H62···O12^{x}		
				H62···O12	2.16	2.09
				N12···O12	2.995 (12)	2.930 (11)
				∠N12H62O12	153	152
O2H1···O4^{v}				O21H11···O41^{xi}		
H1···O4	1.77 (3)	1.76 (2)	1.73 (2)	H11···O41	2.09 (5)	2.14 (5)
O2···O4	2.594 (3)	2.598 (4)	2.563 (4)	O21···O41	2.764 (12)	2.723 (11)
∠O2H1O4	163 (2)	179 (3)	175 (2)	∠O21H11O41	137 (4)	126 (4)
				O22H12···O41^{ix}		
				H12···O41	1.77 (3)	1.71 (3)
				O22···O41	2.593 (9)	2.551 (8)
				∠O22H12O41	167 (3)	176 (4)
N1H5···O3^{vi}				N11H51···O32^{iv}		
H5···O3	1.96	1.97	1.98	H51···O32	2.26	2.22
N1···O3	2.782 (3)	2.779 (5)	2.764 (5)	N11···O32	3.078 (12)	3.041 (10)
∠N1H5O3	149	148	143	∠N11H51O32	149	150
				N12H52···O32^{iv}		
				H52···O32	2.00	1.95
				N12···O32	2.820 (12)	2.774 (11)
				∠N12H52O32	149	150

The molecular geometry of the zwitterions in SPM-II differs significantly from those in SPM-I: Fig. 12 shows an overlay of the benzene rings for phase-I (black) and phase-II (red and yellow). In residue 1 (based on S11, and shown in yellow in Fig. 12) there is a change in the torsion about the S1—C7 vector: τ(O51—S11—C71—C61) changes from 11.6 (3)° to −29.7 (6)° at 2.5 GPa, indicating a rotation of the sulfonate group so that the S11—O51 bond moves away from coplanarity with the ring. In residue 2 (coloured red in Fig. 12), there is a larger rotation of the sulfonate group: τ(O52—S12—C72—C62) = −38.0 (8)° at 2.5 GPa. There is also a change in the torsion about the C32—C42 bond: τ(C52—C42—C32—C22) = 22.7 (11)° at 2.5 GPa, which represents a rotation of the alanine moiety so that the C22—C32 bond is close to the plane of the phenyl ring. This conformational change creates a short intramolecular H···H contact of 1.73 Å (hydrogen distances normalized to standard neutron values).

The change in the molecular conformation has an effect on the packing within layers (Fig. 8*b*). The *C*(9) chains that occur in phase (I) are no longer present in phase (II): two hydrogen bonds are retained throughout the transition (O2H1···O4 = O21H11···O41 and N1H5···O3 = N11H51···O32) and both are *longer* in phase II by *ca* 0.2 and 0.3 Å. Two new discrete hydrogen bonds are formed from carboxyl and ammonium H atoms as a result of the change in conformation of residue 2. These are O22H12···O41 and N12H52···O32; note the symmetry operations for O41 and O32 are different from those in the hydrogen bonds which are retained during the transition (full details are in Table 6). All four interactions combine to make sinusoidal *C*(14) chains which run along the *a* axis.

In addition to the change in packing within the layers, the water molecules between layers change orientation. Fig. 9(*b*) shows how the layers interact with the water molecules; each molecule is coloured according to symmetry equivalence. The water molecules in residue 1 (blue) reorientate so that the hydrogen bonds that were present in phase (I) are broken and new ones are formed to

Table 6 (continued)

Pressure (GPa)	5.2	5.8	6.4	6.9
Phase	(II)	(II)	(II)	(II)
Water–layer hydrogen bonds				
O61H21···O31^{iii}				
H21···O31	2.00 (4)	2.00 (4)	2.00 (3)	1.98 (3)
O61···O31	2.771 (13)	2.767 (13)	2.776 (14)	2.74 (2)
∠O61H21O31	153 (4)	152 (3)	153 (4)	152 (3)
O62H22···O52^{v}				
H22···O52	2.00 (3)	2.02 (3)	1.99 (3)	2.07 (3)
O62···O52	2.797 (16)	2.815 (16)	2.787 (16)	2.87 (2)
∠O62H22O52	159 (4)	159 (4)	159 (4)	159.1 (19)
O61H31...O51^{vi}				
H31···O51	2.07 (3)	2.08 (3)	2.05 (3)	2.04 (3)
O61···O51	2.845 (15)	2.844 (16)	2.822 (16)	2.81 (2)
∠O61H31O51	153 (2)	151 (2)	152 (2)	152 (3)
Water–water hydrogen bonds				
O62H32···O61^{vii}				
H32···O61	2.14 (3)	2.16 (3)	2.16 (3)	2.17 (3)
O62···O61	2.952 (12)	2.962 (11)	2.954 (14)	2.97 (2)
∠O62H32O61	160 (4)	158 (2)	158 (2)	159 (3)
Layer–water hydrogen bonds				
N11H41···O61^{viii}				
H41···O61	1.84	1.84	1.79	1.78
N11···O61	2.713 (16)	2.713 (16)	2.658 (17)	2.65 (2)
∠N11H41O61	160	159	159	160
N12H42···O62^{ix}				
H42···O62	1.94	1.92	1.93	1.83
N12···O62	2.818 (13)	2.794 (12)	2.803 (13)	2.709 (19)
∠N12H42O62	163	162	161	161
N11H61···O62^{ix}				
H61···O62	1.89	1.87	1.88	1.89
N11···O62	2.730 (14)	2.707 (14)	2.711 (15)	2.69 (2)
∠N11H61O62	152	151	151	145
Layer–layer hydrogen bonds				
N12H62···O12^{x}				
H62···O12	2.06	2.05	2.03	2.03
N12···O12	2.898 (11)	2.887 (11)	2.858 (12)	2.809 (16)
∠N12H62O12	153	152	151	142
O21H11···O41^{xi}				
H11···O41	2.09 (4)	2.13 (4)	2.08 (4)	2.08 (3)
O21···O41	2.690 (11)	2.687 (11)	2.667 (11)	2.708 (16)
∠O21H11O41	127 (4)	123 (4)	127 (3)	132 (2)
O22H12···O41^{ix}				
H12···O41	1.70 (3)	1.71 (3)	1.67 (3)	1.698 (19)
O22···O41	2.523 (8)	2.517 (8)	2.501 (9)	2.514 (13)
∠O22H12O41	166 (4)	161 (4)	172 (4)	163 (2)
N11H51···O32^{iv}				
H5···O32	2.21	2.20	2.22	2.34
N11···O32	3.030 (10)	3.025 (11)	3.032 (11)	3.141 (14)
∠N11H51O32	150	150	149	147
N12H52···O32^{iv}				
H52···O32	1.92	1.89	1.89	1.95
N12···O32	2.747 (11)	2.719 (11)	2.713 (11)	2.754 (14)
∠N12H52O32	150	150	149	146

Symmetry codes: (i) $-x, -\frac{1}{2}+y, -z$; (ii) $x, y, 1+z$; (iii) x, y, z; (iv) $1-x, \frac{1}{2}+y, 1-z$; (v) $-x, \frac{1}{2}+y, -z$; (vi) $1-x, -\frac{1}{2}+y, -z$; (vii) $1-x, \frac{1}{2}+y, -z$; (viii) $2-x, \frac{1}{2}+y, 1-z$; (ix) $1-x, -\frac{1}{2}+y, 1-z$; (x) $1-x, \frac{1}{2}+y, 2-z$; (xi) $2-x, -\frac{1}{2}+y, 1-z$.

different molecules. However, the overall orientation still conforms to that in Fig. 1(*a*), with hydrogen bonds formed to layers above and below.

The water molecules in residue two (green) have re-orientated so that all hydrogen bonds are broken except for N1H6···O6 (= N11H61···O62). In this instance, the water molecules are no longer connecting layers through their H atoms: one hydrogen bond is now formed to a sulfonate oxygen in one layer and another is formed to the oxygen on a (residue 1) water molecule.

The most compressible hydrogen bond in SPM-I is O6H2···O4, which is an interaction formed from water molecules to layers. The O···O distance decreases by 3.3% from ambient to 1.0 GPa. The shortest hydrogen bond at 1.0 GPa is a layer–layer interaction: O2H1···O4 [O2···O4 = 2.563 (4) Å], and this is the least compressible hydrogen bond in the structure, shortening by 1.1% at 1.0 GPa relative to ambient conditions.

3.7. Compression of *S*-4-L-phenylalanine monohydrate (II)

Compression of the unit-cell parameters of SPM-II up to a pressure of 6.4 GPa is anisotropic (Fig. 10): the greatest reduction occurred for the *a* axis, and the *b* axis compressed the least.

Above 6.4 GPa, there was a significant drop in the length of the *c* axis from 12.298 (3) to 12.151 (4) Å at 6.9 GPa, and an increase in the length of the *b* axis from 8.1290 (8) to 8.1824 (12) Å. The molecular conformation in residue 2 also changes slightly: the largest changes occur about the C22—C32 bond [τ(N12—C22—C32—C42) = −157.2 (6)° at 6.4 GPa and −165.4 (8)° at 6.9 GPa] and the C42—C92/C52 bonds where the alanine moiety attaches to the phenyl ring [τ(C32—C42—C92—C82) = −170.6 (7)° at 6.4 GPa and −162.8 (11)° at 6.9 GPa]. As the molecular conformation changes, the short intramolecular H···H contact which was formed upon transition becomes longer, from 1.720 Å at 6.4 GPa to 1.789 Å at 6.9 GPa (hydrogen distances normalized to standard neutron values).

The data quality was nowhere near high enough to be able to locate the H atoms, and in the model presented we

have assumed that the orientations of the water molecules remain unchanged during the transition. If this model is correct then there are a number of hydrogen bonds which change abruptly between 6.4 and 6.9 GPa: two hydrogen bonds become markedly longer (O62H22···O52 increases by 0.083 Å and N11H51···O32 increases by 0.109 Å) and one hydrogen bond (N12H42···O62; the least compressible up to 6.4 GPa) becomes significantly shorter from N···O = 2.803 (13) to 2.709 (19) Å.

As pressure is increased on SPM-II, the inter-layer separation decreases from 11.57 to 11.4 Å at 6.4 GPa. Fig. 11 shows that the decrease becomes less rapid as pressure is increased, approaching a minimum at 6.4 GPa before undergoing a marked shortening at 6.9 GPa to 11.32 Å.

4. Discussion

The aim of this paper was to investigate the extent to which the high-pressure phase behaviour of a series of layered hydrates could be predicted on the basis of the orientation of the water molecules. The idea was a simple one: water molecules in the orientation shown in Fig. 3(*a*) limit the scope for layers moving closer together on compression, and the need to reduce volume at high pressure would promote reorientation of the water molecules as shown in Fig. 1(*b*). Just such a transition was observed previously in L-serine monohydrate, and here in SPM, but overall the results of the present study show that matters are a little more complicated. In particular, in none of the structures does the layer stacking direction

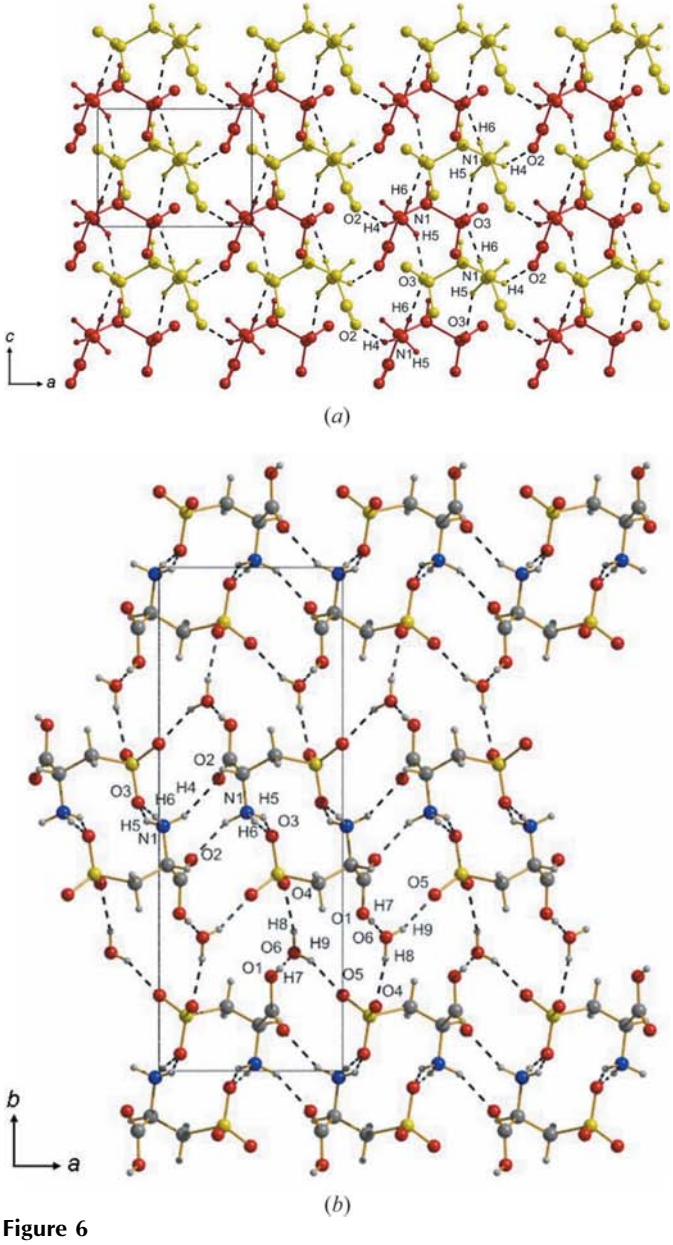

Figure 6
(*a*) One bi-layer of L-cysteic acid molecules viewed along the *b* axis: each half bi-layer is coloured differently for clarity and does not imply crystallographic inequivalence. (*b*) Bi-layers stack along the *b* axis and are separated by layers of water.

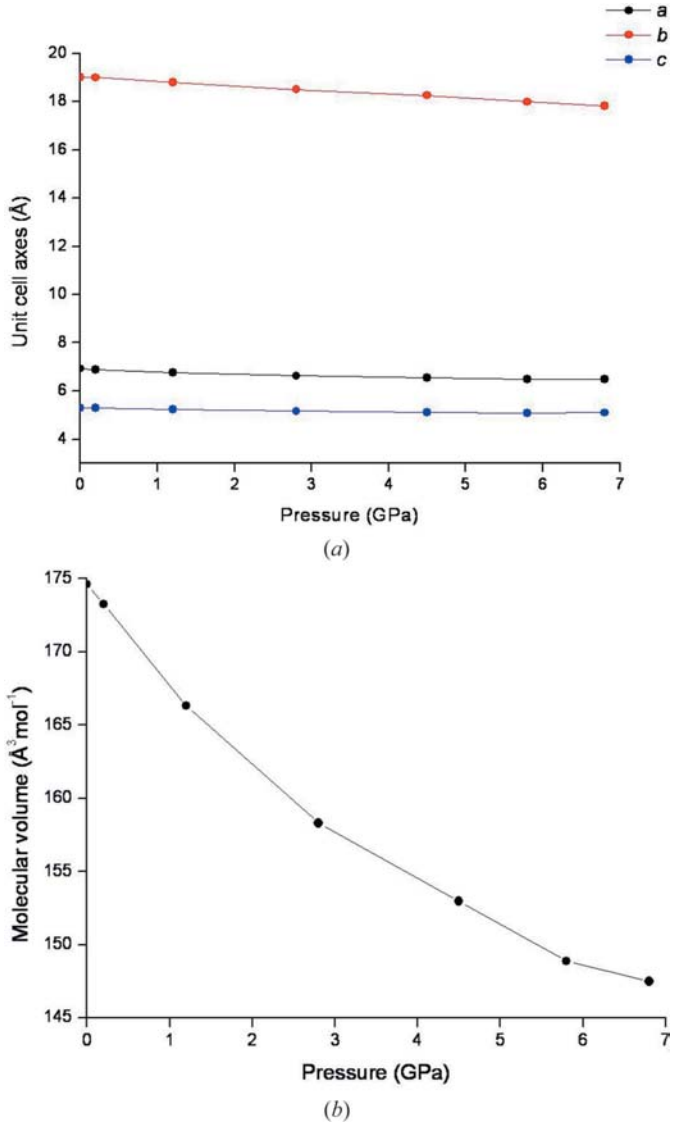

Figure 7
(*a*) Unit-cell axes for L-cysteic acid monohydrate with increasing pressure. (*b*) Molecular volume of L-cysteic acid monohydrate with increasing pressure.

Table 7
Eigenvalues and eigenvectors of the strain tensor for L-serine monohydrate-I and -II, BTM, CAM, SPM-I and -II.

Compound name	Pressure (GPa)	Eigenvalues	Eigenvectors (unit vectors given in the direct axis system)
L-Serine monohydrate (I)	4.5	0.0008 (8)	0.11 0.00 0.00
		−0.0738 (13)	0.00 0.00 0.21
		−0.0983 (7)	0.00 0.08 0.00
L-Serine monohydrate (II)	5.8	−0.0014 (2)	0.10 0.00 0.00
		−0.0043 (2)	0.00 0.00 0.23
		−0.0055 (4)	0.00 0.10 0.00
BTM	7.8	−0.0731 (4)	0.00 0.09 0.00
		−0.0732 (2)	0.11 0.00 0.00
		−0.0915 (2)	0.00 0.00 0.08
CAM	6.8	−0.0386 (2)	0.00 0.00 0.19
		−0.0625 (1)	0.00 0.05 0.00
		−0.0628 (2)	0.14 0.00 0.00
SPM-I	1.0	−0.0085 (1)	0.08 0.00 0.08
		−0.0220 (1)	0.00 0.13 0.00
		−0.0279 (1)	0.13 0.00 −0.04
SPM-II	6.4	−0.0115 (3)	0.07 0.00 0.08
		−0.0142 (1)	0.00 0.12 0.00
		−0.0619 (1)	0.09 0.00 −0.02

correspond to the direction of greatest linear strain. However, the reasons for the differences between the effects of pressure on serine hydrate, BTM, CAM and SPM, can be understood by consideration of (*a*) hydrogen-bonding directions and (*b*) void distributions.

Hydrogen bonds are amongst the strongest of all intermolecular interactions, they are strongly directional, and, although much depends on the shape of the potential in each specific case, strong hydrogen bonds will tend to inhibit compression along parallel directions in a crystal. For example, amino acids typically form head-to-tail hydrogen-bonded chains of molecules, and the chain direction is usually found to have the smallest linear strain under pressure (Dawson *et al.*, 2005; Moggach *et al.*, 2005; Johnstone *et al.*, 2008). Similar conclusions have been reached for chloropyridinium tetrachloro- and bromo-cobaltate (Espallargas *et al.*, 2008).

An alternative guide to distortions at high pressure is the distribution of interstitial voids. In previous publications (Moggach *et al.*, 2005; Wood *et al.*, 2006), void analysis using Voronoi–Dirichlet polyhedra (Blatov & Shevchenko, 2003) has been found to be useful in the identification of the size and distribution of voids within a crystal structure. It was observed that there is a correlation between the positions of the largest voids within the structure and the directions of compression. Void distributions can also be investigated using recently added features in *Mercury* (Macrae *et al.*, 2008).

In serine hydrate the eigenvalues and vectors of the strain tensor at 4.5 GPa are given in Table 7. The numerically smallest strain is along **a**, the direction of head-to-tail chains of molecules. Fig. 13 shows the void distribution at ambient conditions, 4.5 (just before phase transition) and 5.2 GPa (just after phase transition). At ambient conditions, the voids are distributed more-or-less evenly within and between the layers of serine molecules (shown in black, water molecules are red). Compression to 4.5 GPa, results in a significant reduction in the size of all voids in the structure, and this occurs by compression along the **b** and **c** directions. The hydrogen bonds formed by the water molecules to serine (approximately in the *b* direction) are weaker than those formed between serine molecules, and as a result the layer-stacking *b* direction experiences a slightly greater linear strain than the *c* direction. Above 5 GPa the structure transforms to a new phase, a transition that involves re-orientation of the water molecules

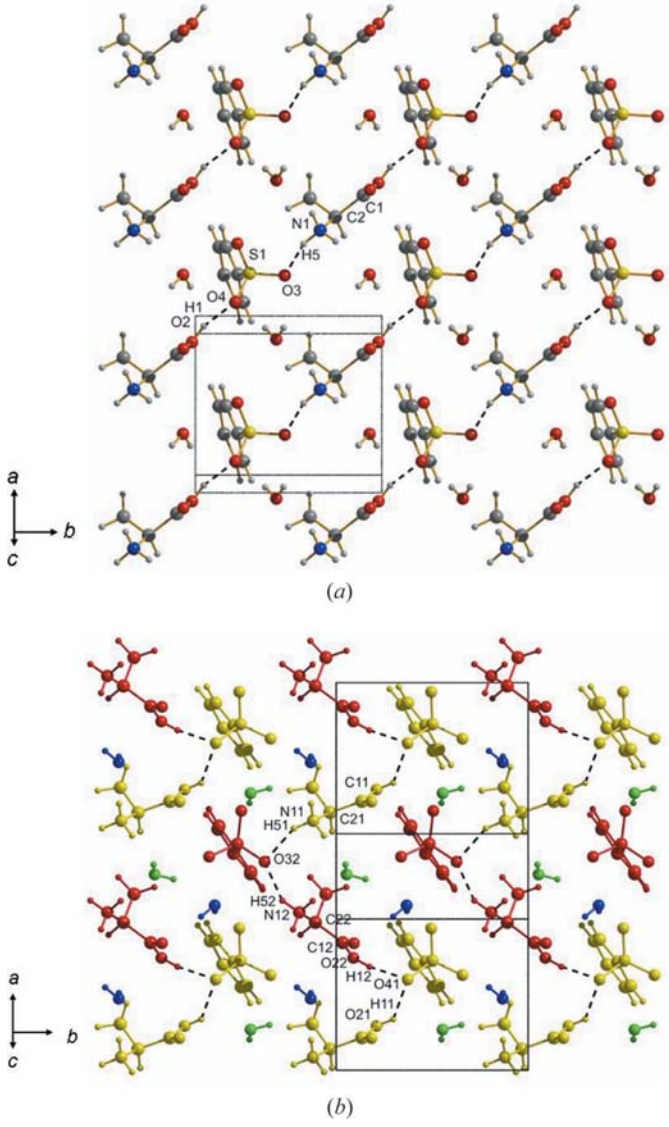

Figure 8
Layers of (*a*) *S*-4-sulfo-L-phenylalanine monohydrate (I) and (*b*) (II) viewed approximately along the reciprocal *c** axis to show the hydrogen bonding within layers. Each molecule is cropped at the C3—C4 bond and hydrogen bonding to water has been omitted for clarity. In (*b*) the molecules are coloured by symmetry equivalence: residue 1 is yellow or blue, and residue 2 is red or green.

and a reduction in the inter-layer stacking distance. Interestingly this seems to create small voids within the water layers; these disappear as pressure is increased.

Fig. 14 shows the distribution of voids in BTM at ambient pressure, 4.0 and 7.8 GPa. The voids are quite uniformly distributed within the structure, and compression is significant along all three principal directions (the range of linear strain is −0.07 to −0.09, Table 7). The layer-stacking direction (*b*) corresponds to the direction of hydrogen-bond formation, and is the least compressible.

By 4.0 GPa the voids in the water layers have closed, a factor which appears to be correlated with a change in the behaviour of the sinusoidal betaine and water layers (Fig. 4*b*). At ambient pressure both layers are slightly sinusoidal, and up to 4.0 GPa an increase in pressure increases the amplitude of the modulation. In the case of the betaine layers the modulation can be quantified using the separation between layers calculated using the red and blue molecules in Fig. 4(*b*); a similar calculation can be carried out for the green and yellow water molecules. These changes can also be visualized in the form of a movie, which has been deposited as supplementary material (Movie 1).

The variation in the two modulation distances with pressure is shown in Figs. 15(*a*) and (*b*). In Fig. 15(*a*) there is a clear transition point from 4.0 to 4.9 GPa where the plane separation remains constant before continuing to increase again. Fig. 15(*b*), by contrast, proceeds through a distinct maximum at 4.9 GPa. All void space has effectively closed up by 7.8 GPa.

The path of compression in BTM is clearly not uniform, but at no stage does the structure transform to a new phase: this is

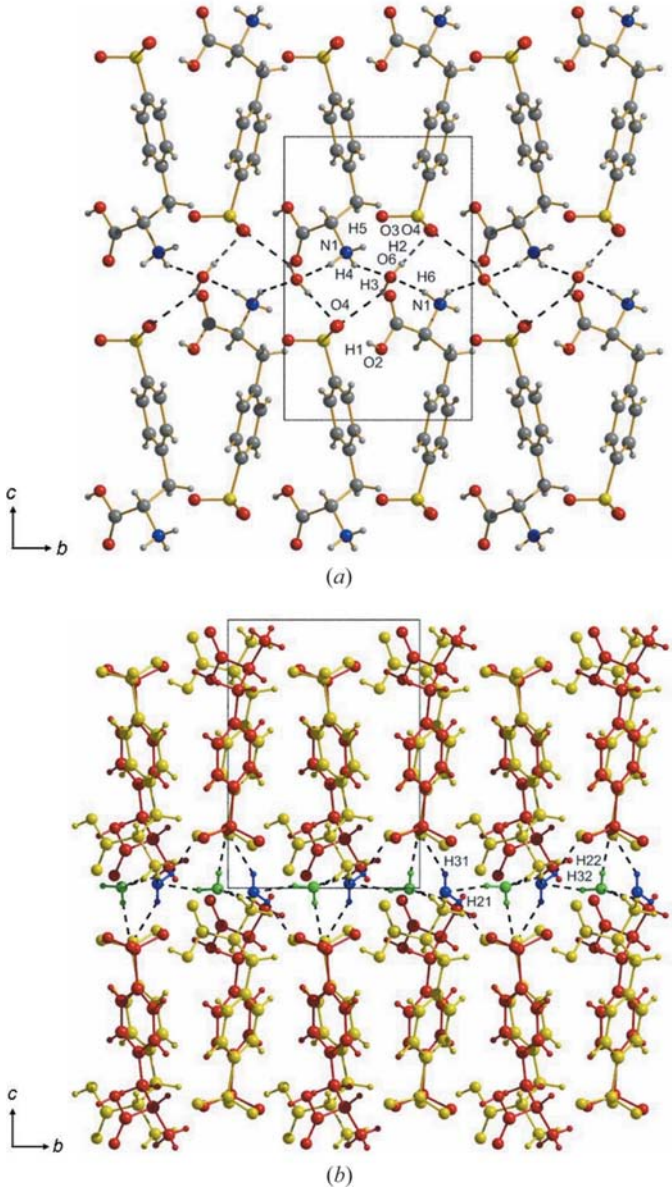

Figure 9
Layers of *S*-4-sulfo-L-phenylalanine monohydrate viewed along the crystallographic *a* axis for (*a*) SPM-I and (*b*) SPM-II. Hydrogen bonding within layers has been omitted for clarity. In (*b*) the molecules are coloured by symmetry equivalence: residue 1 is yellow or blue and residue 2 is red or green.

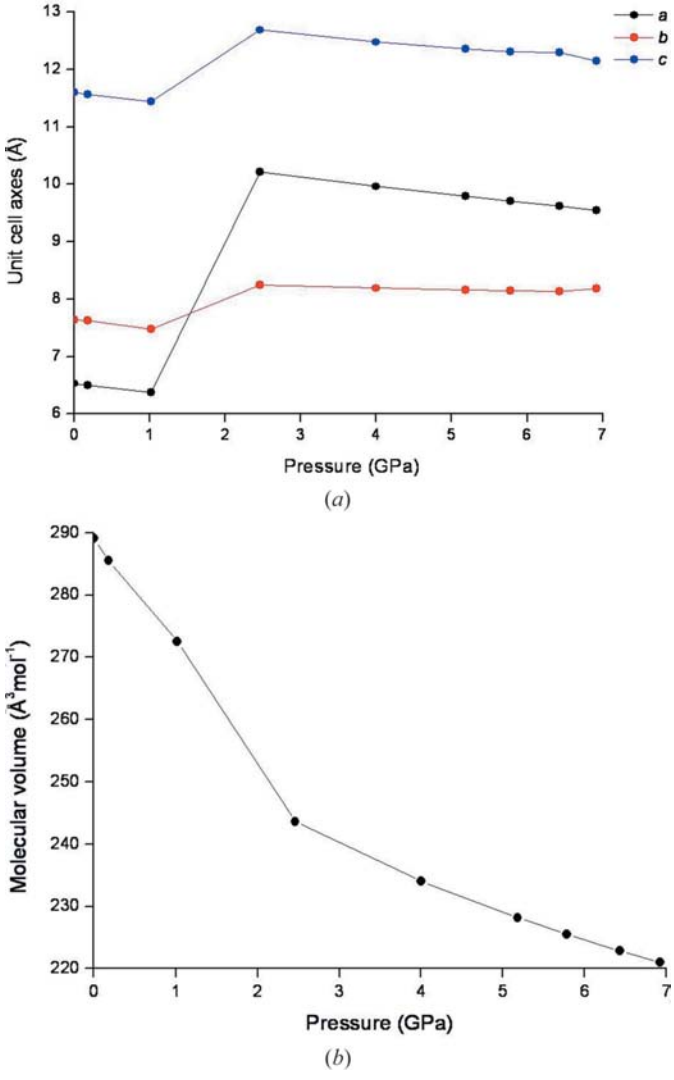

Figure 10
(*a*) Unit cell axes for *S*-4-sulfo-L-phenylalanine monohydrate with increasing pressure. (*b*) Molecular volume of *S*-4-sulfo-L-phenylalanine monohydrate with increasing pressure.

highlighted in Fig. 16 where the *normalized holistic r.m.s. deviation* (a packing-similarity tool available in *Mercury*) for the three hydrates is plotted against pressure. For BTM, it is apparent that the largest change in packing occurs within the first few GPa, and after this there is very little change.

The least compressible direction in CAM is the *c* direction, which is parallel to strong $NH_3^+\cdots SO_3^-$ hydrogen bonds which build the bi-layers of cysteic acid molecules. When strain is calculated using the cell-dimension data at 6.8 GPa (Table 7) the *a* and *b* axes appear to be equally compressible. A movie showing the compression of the structure viewed along the *c* axis is available in the supplementary material (Movie 2). The compression along the **a** direction causes the alignment of pairs of cysteic acid molecules in the bi-layers to become more parallel to the **b** direction as the voids between them decrease in size (compare the movie with the void distributions shown in Fig. 17). At the same time the distance between the bi-layers decreases and the rows of water molecules become less sinusoidal. Between ambient pressure and 5.8 GPa the linear strain along the *a* axis is greater than along *b* (Fig. 18), a difference also reflected in the void distributions shown in Fig. 17: the voids located in the bi-layers are compressed along the **a** direction more quickly than the extended voids which exist in the water layers are compressed along **b**.

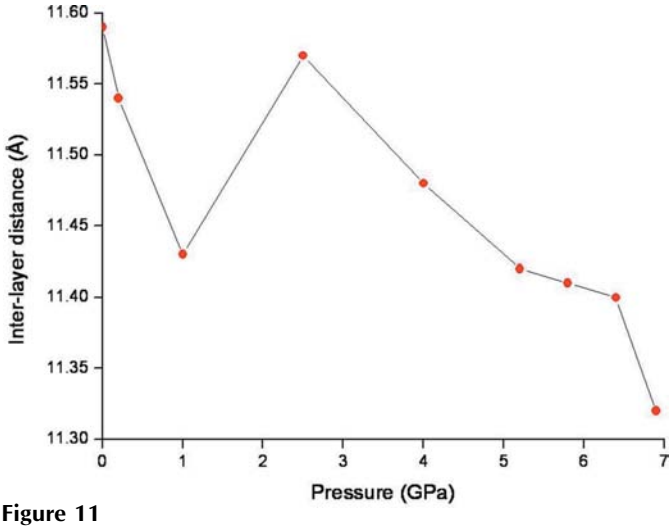

Figure 11
Separation between layers of zwitterions in both phases of *S*-4-sulfo-L-phenylalanine monohydrate with increasing pressure. The layers of zwitterions are parallel to the (001) planes and formed by lattice repeats along *c*, and for the purposes of this figure the interlayer distance is equated with d_{001} (= $1/c^*$).

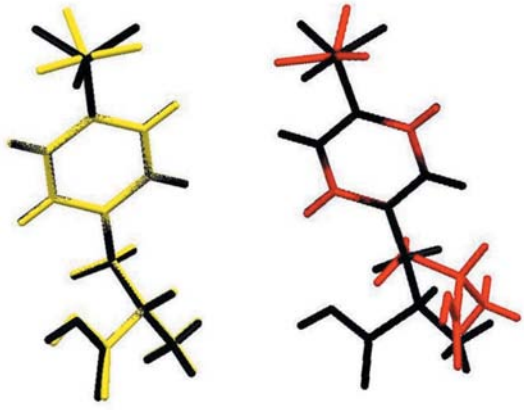

Figure 12
Overlay of phase (I) (black molecules) and phase (II) (red and yellow molecules are residues 1 and 2) in *S*-4-sulfo-L-phenylalanine monohydrate.

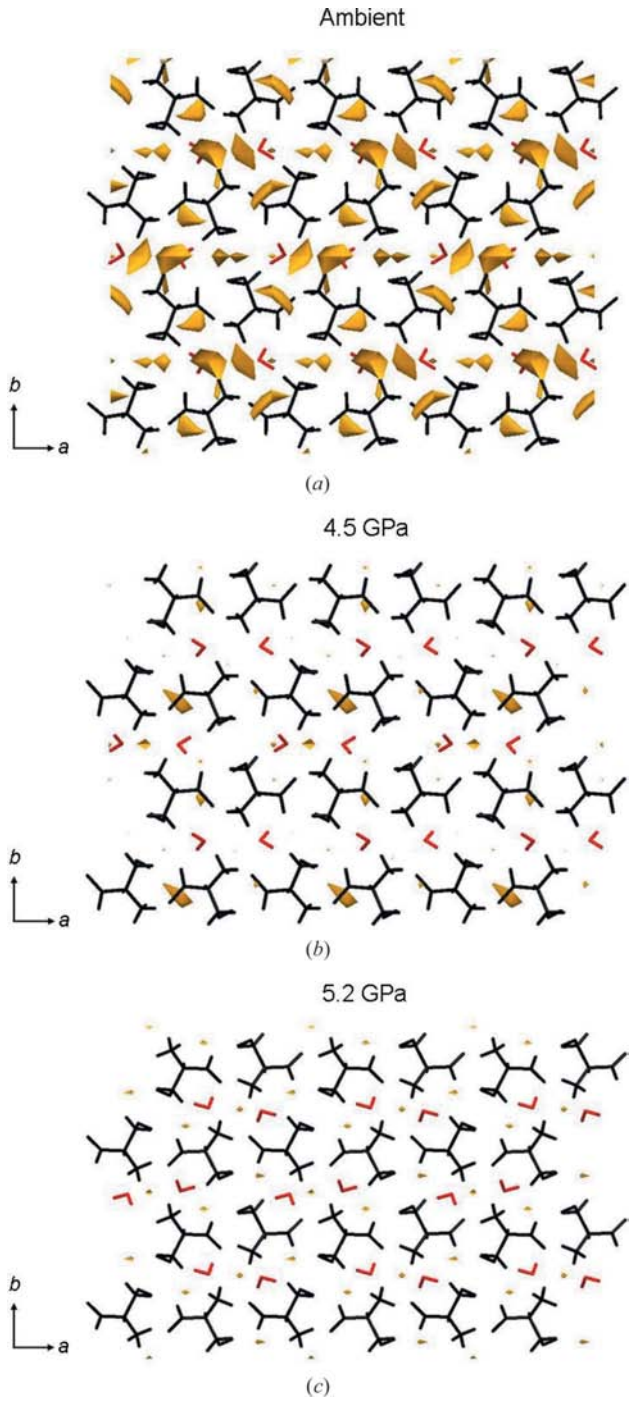

Figure 13
Void distribution in L-serine monohydrate at ambient conditions, 4.5 and 5.2 GPa. Four layers of serine run vertically down the page: serine molecules are shown in black, and water molecules are shown in red.

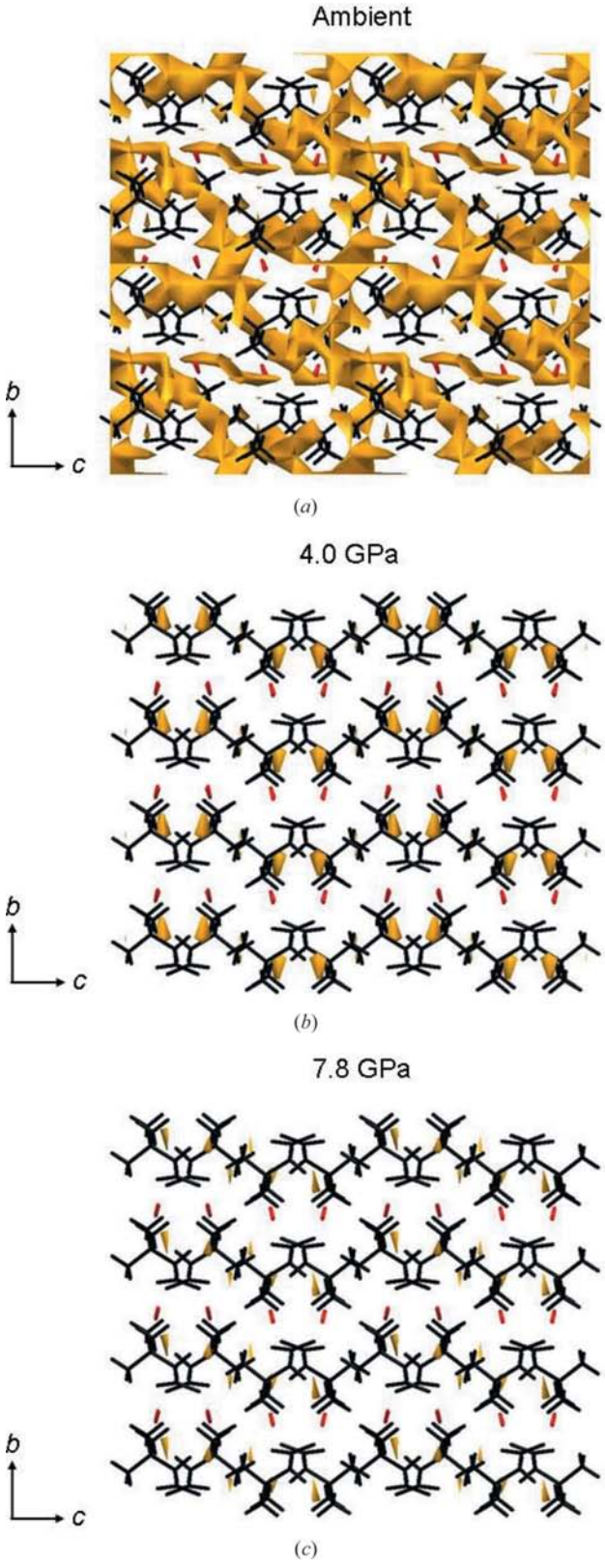

Figure 14
Void distribution in betaine monohydrate at ambient conditions, 4.0 GPa and at a final pressure of 7.8 GPa. Four layers of betaine molecules run vertically down the page: betaine molecules are shown in black, and water molecules are shown in red.

With reference to Fig. 16, it can be seen that the packing in CAM does not change much throughout the compression study, and as in BTM, most of the compression occurs in the initial stages when the intermolecular interactions are less repulsive.

The structure of SPM-I is characterized by elongated voids which run approximately along the *ac* diagonal (Fig. 19*a*). The largest component of the strain tensor lies along the [0.13 0.00 −0.04] direction; indicated with a red arrow in Fig. 19(*a*), which lies perpendicular to the long dimension of the voids. One of the principal axes of the strain tensor must lie along the *b* axis by symmetry: the strain along this direction is only a little smaller than along [0.13 0.00 −0.04]. The third strain axis makes a right-handed set, lying along [0.08 0.00 0.08], approximately along the length of the voids.

The response of SPM to pressure, as viewed along the *b* axis, is depicted in the form of a movie in the supplementary

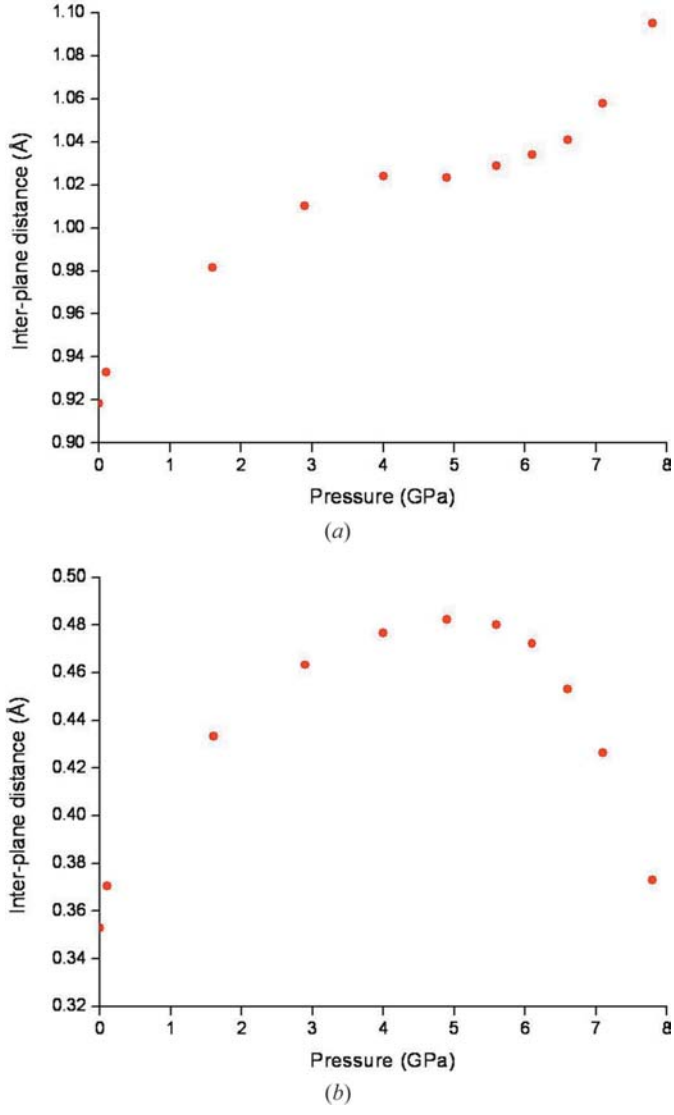

Figure 15
Inter-plane separation in betaine monohydrate for (*a*) betaine layers and (*b*) water layers.

material (Movie 3). Even though the precise directions of greatest compression are not necessarily very obvious in the movie, it is clear that the structure compresses most in the horizontal direction. The phase transition which occurs above 1 GPa can be seen as a more abrupt compression in this same direction. The trend persists after the phase transition, and the exact directions of greatest and least strain are illustrated in Fig. 19(*b*).

A common feature in high-pressure studies of layered structures is that the greatest amount of compression occurs along the layer stacking direction: this does not occur in SPM.

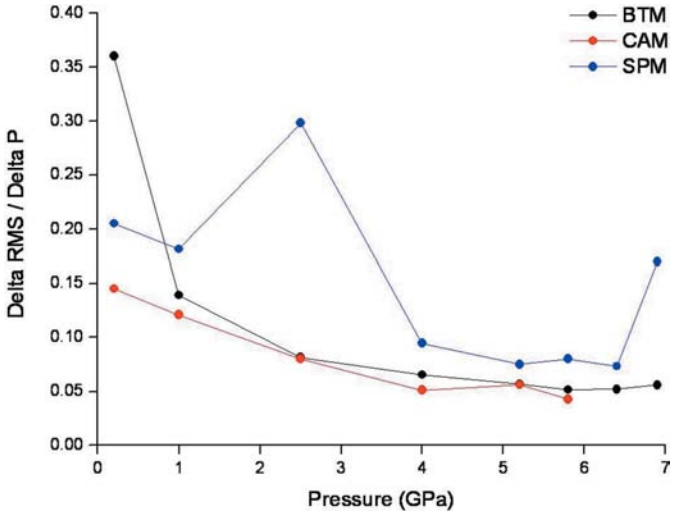

Figure 16
Graph showing the normalized holistic r.m.s. deviation for BTM, CAM and SPM as a function of pressure.

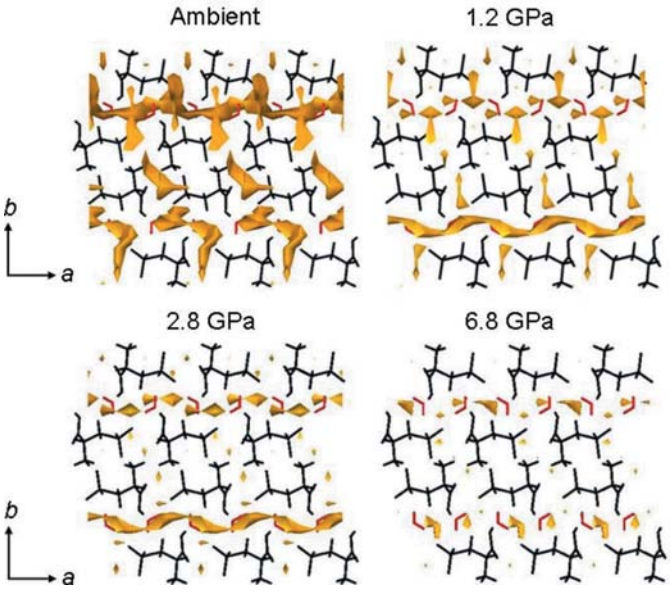

Figure 17
Void distribution in L-cysteic acid monohydrate at increasing pressures: L-cysteic acid molecules are shown in black, and water molecules are shown in red.

Part of the reason for this can be traced to the shapes of the voids, but, in addition, this direction is also parallel to the strongest interactions in the structure, namely the hydrogen bonds formed between the layers, and the lengths of the molecules. Rather than decrease the layer-stacking distance during the phase transition (as occurs in serine hydrate), the layers actually move further apart, almost as though the system of hydrogen bonds formed between the layers is acting like a compressed spring.

In other respects the transitions in serine hydrate and SPM are quite similar: in both cases water molecules reorient, hydrogen bonding within the layers of zwitterions is disrupted and the zwitterions themselves change conformation.

At 6.9 GPa there is a discontinuity in the cell dimensions of SPM-II *versus* pressure plots, and in the layer-stacking distance plot shown in Fig. 11. There are no significant reorientations in the *S*-4-sulfo-L-phenylalanine molecules, although there is a modest change in torsion angle which appears to relieve a short intramolecular H···H contact. We cannot make a definitive statement about the orientations of the water molecules as H atoms could not be located precisely.

Fig. 16 shows the distinct change in packing when the phase transition occurs in SPM at 1 GPa. It is also interesting to see that there is a significant change between the structures at 6.4 and 6.9 GPa when the discontinuity in the cell dimensions occurs.

4.1. Driving force of the transition

The character of the phase transition in SPM has similarities to serine hydrate: as pressure is increased on phase (I), layers approach one another, and as the transition occurs hydrogen bonding within layers is disrupted as the geometry of the zwitterions changes. The water molecules also change their orientation, although this is not to allow further approach of

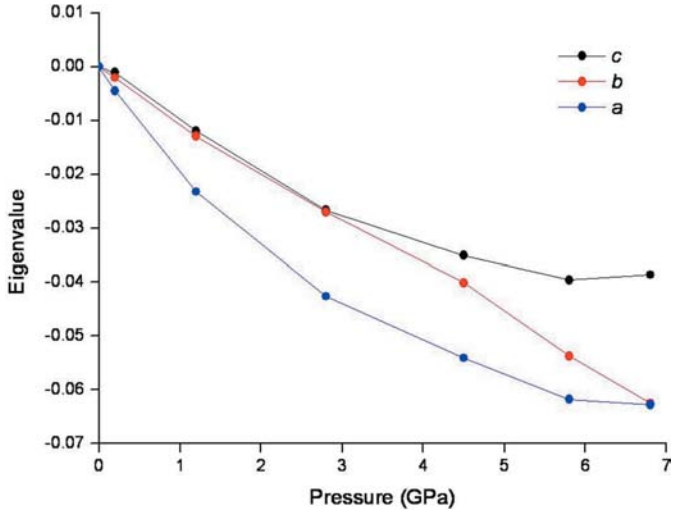

Figure 18
Eigenvaules of the strain tensor for L-cysteic acid monohydrate with increasing pressure.

the layers: the layers move further apart through the transition (Fig. 11).

SPM-I contains a very short hydrogen bond [O2H1···O4, O···O = 2.563 (4) Å at 1.0 GPa], and a search of the Cambridge Crystallographic Database for *R*COOH to RSO_3^- interactions reveals that there are no structures where O···O distances appear to be shorter than this [the shortest occurs in VOJGAC where O···O = 2.561 (3) Å]. PIXEL calculations performed on SPM-I indicate that despite the close proximity of the O atoms, this interaction is strongly stabilizing at ambient conditions and becomes even more so upon compression to 1.0 GPa. Similar comments could be made about intermolecular interaction energies in serine and serine hydrate, which are also zwitterionic. In phase (II) the interaction becomes even shorter: O22···O42 = 2.514 (13) Å at 6.9 GPa. It is not possible to carry out PIXEL calculations on this structure as there are too many molecules in the asymmetric unit, but we do not see any convincing evidence from the intermolecular distances that would lead us to conclude that the transition is driven by relief of repulsive intermolecular contacts.

The molecular volume decreases significantly throughout the transition (Fig. 10*b*). Extrapolation of the phase (I) points indicates that the molar volume of SPM-II at 2.5 GPa is *ca* 6 $Å^3$ mol^{-1} lower than a hypothetical phase (I) structure at the same pressure. This equates to a *PV* energy of 9 kJ mol^{-1}, indicating that, as in serine and serine hydrate; the *PV* term is an important factor determining the driving force of the transition.

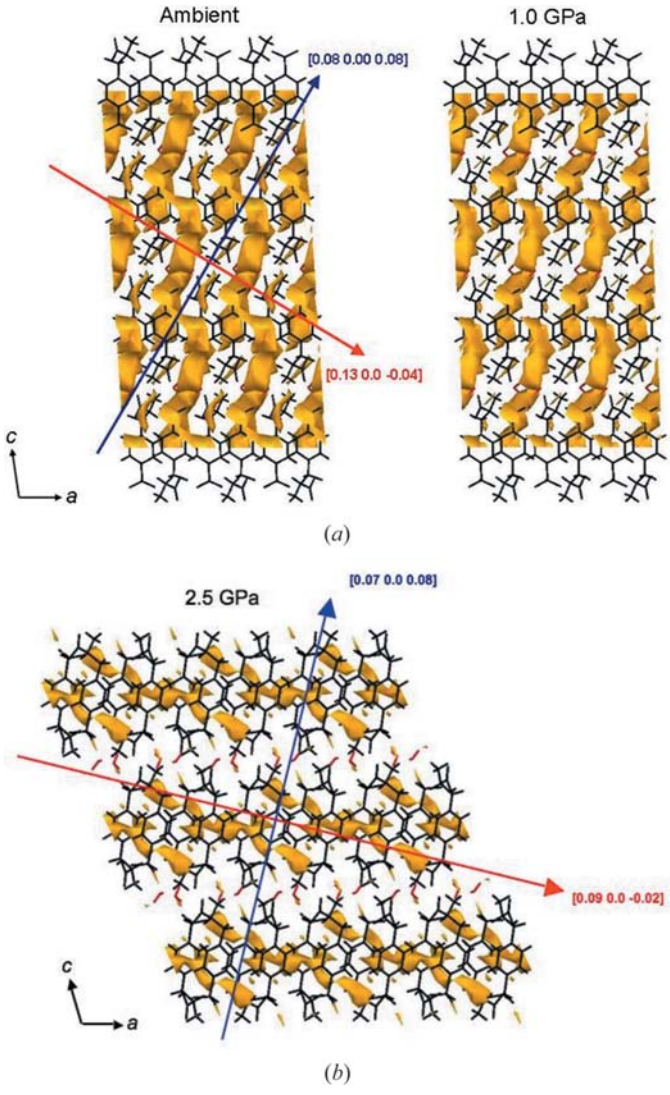

Figure 19
Void distribution in (*a*) SPM-I at ambient conditions and 1.0 GPa, and (*b*) SPM-II at 2.5 GPa. *S*-4-Sulfo-L-phenylalanine molecules are shown in black, and water molecules are shown in red. Red and blue arrows indicate the directions of greatest and least strain (*cf* Table 7).

5. Conclusions

We have described the effects of pressure on the crystal structures of betaine monohydrate, L-cysteic acid monohydrate and *S*-4-sulfo-L-phenylalanine monohydrate using single-crystal synchrotron X-ray diffraction. In all cases, the least amount of compression was found to occur along the directions where hydrogen bonds form; and the largest amount of compression occurred along the directions of large voids present within the structure.

A single-crystal to single-crystal phase transition occurs in *S*-4-sulfo-L-phenylalanine monohydrate at pressures above 1.0 GPa. In common with the phase transition in serine hydrate the SPM-I to -II transition is characterized by:

(i) a change in the conformation of the layer-building molecules and

(ii) reorientation of the water molecules between layers.

The original contention was that the water molecules would change their orientation in order to facilitate further shortening of the inter-layer distance: this did not occur, and in fact the layers moved further apart. In other respects the transitions in serine hydrate and SPM are more similar: the water molecules reorient, the zwitterions change conformation and hydrogen bonding within the zwitterionic layers is disrupted.

By analogy with the phase transition in serine hydrate, it is possible that the transition in SPM is driven by the need to increase packing efficiency at high pressure. Above 6.4 GPa, there is a break in the trend of the unit-cell parameters: the *b* axis increases whilst the *a* axis decreases, and as this happens the inter-layer separation reduces significantly and a short *intra*molecular H···H contact is lengthened.

We thank the EPSRC and The Cambridge Crystallographic Data Centre for funding and STFC for provision of synchrotron beam-time. We also thank Dr Lukas Palatinus (EPFL Lausanne) for his help with calculations using BAYMEM. Finally, we thank Dr Stephen Moggach, Mr Pascal Parois and Mr Alessandro Prescimone for their help with the synchrotron experiments.

References

Allan, D. R. & Clark, S. J. (1999*a*). *Phys. Rev. B*, **60**, 6328–6334.

Allan, D. R. & Clark, S. J. (1999*b*). Phys. Rev. Lett. **82**, 3464–3467.

Allan, D. R., Clark, S. J., Brugmans, M. J. P., Ackland, G. J. & Vos, W. L. (1998). *Phys. Rev. B*, **58**, R11809–R11812.

Allan, D. R., Clark, S. J., Dawson, A., McGregor, P. A. & Parsons, S. (2002). *Acta Cryst.* B**58**, 1018–1024.

Allan, D. R., Clark, S. J., Ibberson, R. M., Parsons, S., Pulham, C. R. & Sawyer, L. (1999). *Chem. Commun.* **8**, 751–752.

Allan, D. R., Parsons, S. & Teat, S. J. (2001). *J. Synchrotron Rad.* **8**, 10–17.

Allen, F. H. & Motherwell, W. D. S. (2002). *Acta Cryst.* B**58**, 407–422.

Altomare, A., Cascarano, G., Giacovazzo, C., Guagliardi, A., Burla, M. C., Polidori, G. & Camalli, M. (1994). *J. Appl. Cryst.* **27**, 435.

Bernstein, J., Davis, R. E., Shimoni, L. & Chang, N.-L. (1995). *Angew. Chem. Int. Ed. Engl.* **34**, 1555–1573.

Betteridge, P. W., Carruthers, J. R., Cooper, R. I., Prout, K. & Watkin, D. J. (2003). *J. Appl. Cryst.* **36**, 1487.

Blatov, V. A. & Shevchenko, A. P. (2003). *Acta Cryst.* A**59**, 34–44.

Blessing, R. H. (1987). *Crystallogr. Rev.* **1**, 3–58.

Boldyreva, E. V., Shakhtshneider, T. P., Ahsbahs, H., Sowa, H. & Uchtmann, H. (2002). *J. Therm. Anal. Calorim.* **68**, 437–452.

Boldyreva, E. V., Shakhtshneider, T. P., Vasilchenko, M. A., Ahsbahs, H. & Uchtmann, H. (2000). *Acta Cryst.* B**56**, 299–309.

Brandenburg, K. & Putz, H. (2005). *DIAMOND*, Version 3.2. Crystal Impact GbR, Bonn, Germany.

Bruker–Nonius (2006). *SAINT*, Version 7. Bruker AXS, Madison, Wisconsin, USA.

Burla, M. C., Caliandro, R., Camalli, M., Carrozzini, B., Cascarano, G. L., De Caro, L., Giacovazzo, C., Polidori, G. & Spagna, R. (2005). *J. Appl. Cryst.* **38**, 381–388.

Dawson, A., Allan, D. R., Belmonte, S. A., Clark, S. J., David, W. I. F., McGregor, P. A., Parsons, S., Pulham, C. R. & Sawyer, L. (2005). *Cryst. Growth Des.* **5**, 1415–1427.

Dawson, A., Allan, D. R., Parsons, S. & Ruf, M. (2004). *J. Appl. Cryst.* **37**, 410–416.

Espallargas, G. M., Brammer, L., Allan, D. R., Pulham, C. R., Robertson, N. & Warren, J. E. (2008). *J. Am. Chem. Soc.* **130**, 9058–9071.

Fabbiani, F. P. A. & Pulham, C. R. (2006). *Chem. Soc. Rev.* **35**, 932–942.

Farrugia, L. J. (1999). *J. Appl. Cryst.* **32**, 837–838.

Flack, H. D. (1983). *Acta Cryst.* A**39**, 876–881.

Frisch, M. J. *et al.* (1998). *GAUSSIAN*98, Revision A.7. Gaussian, Inc., Pittsburgh, PA, USA.

Gavezzotti, A. (2003). *OPIX*. University of Milano, Milan, Italy.

Gavezzotti, A. (2005). *Z. Kristallogr.* **220**, 499–510.

Gavezzotti, A. (2007). *Molecular Aggregation: Structure Analysis and Molecular Simulation of Crystals and Liquids.* Oxford University Press.

Hazen, R. M. & Finger, L. W. (1982). *Comparative Crystal Chemistry: Temperature, Pressure, Composition and the Variation of Crystal Structure*, p. 81. Chichester, New York, USA: John Wiley and Sons.

Johnstone, R. D. L., Francis, D., Lennie, A. R., Marshall, W. G., Moggach, S. A., Parsons, S., Pidcock, E. & Warren, J. E. (2008). *CrystEngComm*, **10**, 1758–1769.

Larson, A. C. (1970). *Crystallographic Computing*, pp. 291–294. Copenhagen: Munksgaard.

Macrae, C. F., Bruno, I. J., Chisholm, J. A., Edgington, P. R., McCabe, P., Pidcock, E., Rodriguez-Monge, L., Taylor, R., van de Streek, J. & Wood, P. A. (2008). *J. Appl. Cryst.* **41**, 466–470.

Mak, T. C. W. (1990). *J. Mol. Struct.* **220**, 13–18.

Merrill, L. & Bassett, W. A. (1974). *Rev. Sci. Instrum.* **45**, 290–294.

Moggach, S. A., Allan, D. R., Morrison, C. A., Parsons, S. & Sawyer, L. (2005). *Acta Cryst.* B**61**, 58–68.

Moggach, S. A., Allan, D. R., Parsons, S. & Warren, J. E. (2008). *J. Appl. Cryst.* **41**, 249–251.

Moggach, S. A., Parsons, S. & Wood, P. A. (2008). *Cryst. Rev.* **14**, 143–184.

Oswald, I. D. H., Allan, D. R., Day, G. M., Motherwell, W. D. S. & Parsons, S. (2005). *Cryst. Growth Des.* **5**, 1055–1071.

Oswald, I. D. H., Allan, D. R., Motherwell, W. D. S. & Parsons, S. (2005). *Acta Cryst.* B**61**, 69–79.

Parsons, S. (2003). *STRAIN*. University of Edinburgh, UK.

Parsons, S. (2004). *SHADE*. The University of Edinburgh, UK.

Piermarini, G. J., Block, S., Barnett, J. D. & Forman, R. A. (1975). *J. Appl. Phys.* **46**, 2774–2780.

Prescimone, A., Milios, C. J., Moggach, S. A., Warren, J. E., Lennie, A. R., Sanchez-Benitez, J., Kamenev, K., Bircher, R., Murrie, M., Parsons, S. & Brechin, E. K. (2008). *Angew. Chem. Int. Ed.* **47**, 2828–2831.

Press, W. H., Teukolsky, S. A., Vetterling, W. T. & Flannery, B. P. (1992). *Numerical Recipes in Fortran*, 2nd Ed. Cambridge University Press.

Prince, E. (1982). *Mathematical Techniques in Crystallography and Materials Science.* New York: Springer-Verlag.

Ramanadham, M., Sikka, S. K. & Chidambaram, R. (1973). *Acta Cryst.* B**29**, 1167–1170.

Sheldrick, G. M. (2004). *SADABS*, Version 2004–1. Bruker-AXS, Madison, Wisconsin, USA.

Sheldrick, G. M. (2005). *SHELXTL-XP*. University of Göttingen, Germany, and Bruker–Nonius, Madison, Wisconsin, USA.

Siemens (1996). *SADABS*. Siemens Analytical X-ray Instruments Inc., Madison, Wisconsin, USA.

Smaalen, S. van, Palatinus, L. & Schneider, M. (2003). *Acta Cryst.* A**59**, 459–469.

Spek, A. L. (2004). *PLATON*. Utrecht University, The Netherlands.

Watkin, D. (1994). *Acta Cryst.* A**50**, 411–437.

Watkin, D. J., Pearce, L. & Prout, K. (1993). *CAMERON*. Chemical Crystallography Laboratory, University of Oxford, UK.

Wood, P. A., Forgan, R. S., Henderson, D., Parsons, S., Pidcock, E., Tasker, P. A. & Warren, J. E. (2006). *Acta Cryst.* B**62**, 1099–1111.

Wood, P. A., Francis, D., Marshall, W. G., Moggach, S. A., Parsons, S., Pidcock, E. & Rohl, A. L. (2008). *CrystEngComm*, **10**, 1154–1166.

Xie, Y.-R., Xiong, R.-G., Xue, X., Chen, X.-T., Xue, Z. & You, X.-Z. (2002). *Inorg. Chem.* **41**, 3323–3326.